



## Recycling deep cratonic lithosphere and generation of intraplate magmatism in the North China Craton

Shan Gao <sup>a,b,\*</sup>, Roberta L. Rudnick <sup>c</sup>, Wen-Liang Xu <sup>d</sup>, Hong-Lin Yuan <sup>b</sup>, Yong-Sheng Liu <sup>a</sup>, Richard J. Walker <sup>c</sup>, Igor S. Puchtel <sup>c</sup>, Xiaomin Liu <sup>b</sup>, Hua Huang <sup>a</sup>, Xiao-Rui Wang <sup>a</sup>, Jie Yang <sup>a</sup>

<sup>a</sup> State Key Laboratory of Geological Processes and Mineral Resources, China University of Geosciences, Wuhan 430074, China

<sup>b</sup> State Key Laboratory of Continental Dynamics, Department of Geology, Northwest University, Xi'an 710069, China

<sup>c</sup> Geochemistry Laboratory, Department of Geology, University of Maryland College Park, MD 20742, USA

<sup>d</sup> School of Earth Sciences, Jilin University, Changchun 130061, China

### ARTICLE INFO

#### Article history:

Received 30 September 2007

Received in revised form 22 February 2008

Accepted 1 March 2008

Available online 13 March 2008

Editor: R.W. Carlson

#### Keywords:

upper mantle  
lower crust  
foundering  
delamination  
basalt  
picrite  
North China craton

### ABSTRACT

Early Cretaceous alkaline picrites and high-magnesium basalts from the North China craton provide evidence for recycling of continental lithosphere by density foundering. Both the picrites and basalts contain xenocrystic olivines with high  $Fo_{92-93}$  and low CaO (<0.10%), consistent with the lavas' derivation from, or interaction with Archean mantle lithosphere. Most importantly, both the picritic and basaltic lavas contain unusual, reversely zoned clinopyroxene phenocrysts whose cores have low MgO, high Na<sub>2</sub>O (up to 2.4 wt.%, or 17.3 mol% Jd), and frequently contain ilmenite exsolution lamellae, consistent with their crystallization from an eclogite-derived melt (tonalite or trondhjemite). In contrast, the clinopyroxene exteriors have low Na<sub>2</sub>O (<0.92 wt.%, or <6.5 mol% Jd) and are lamellae-free, suggesting crystallization from a mantle-derived melt (picrite or basalt). Both the cores and exteriors have high Al<sub>2</sub>O<sub>3</sub> contents (up to 6.9 wt.%). These features reflect crystallization of the cpx from an aluminous melt at mantle depths, with the cores forming at a significantly greater depth ( $\geq 2.5$  GPa) than the surrounding cpx ( $\geq 1.5$  GPa). Calculated primary melt compositions further constrain the magmas' formation at 3–4 GPa, in the presence of garnet. The unusually low CaO, high Ni/MgO and low 100Mn/Fe of primary melts indicate derivation of both the picritic and basaltic lavas from pyroxenite sources containing limited or no olivine. High Sr/Y, La<sub>N</sub>/Yb<sub>N</sub> and Th/U and low Lu/Hf, together with radiogenic initial  $^{87}\text{Sr}/^{86}\text{Sr}$  and  $^{187}\text{Os}/^{188}\text{Os}$  ratios and negative  $\epsilon_{\text{Nd}}$  values implicate contributions from melts derived from foundered eclogitic lower continental crust. Modelling suggests that the basalt source region contained a variable proportion (30–40%) of eclogite-derived component whereas the source of the picrites, on average, likely contained a generally higher proportion (60–70%) of a different eclogite-derived component.

Collectively, these results suggest that both the basaltic and picritic lavas originated by partial melting of Archean lithospheric mantle that was variably hybridised by melts derived from foundered lower crustal eclogite. Together with previous studies, these findings provide new evidence that thinning of the North China craton was caused by the removal of the lower lithosphere (mantle and lower crust). Recycling and melting of eclogitic lower crust may contribute more to mantle heterogeneity than has previously been recognized.

© 2008 Elsevier B.V. All rights reserved.

### 1. Introduction

Recycling of eclogite of lower continental crust origins, together with the underlying lithospheric mantle, has been proposed to play a role in plume magmatism, crustal evolution and formation of chemical heterogeneities within the mantle (Arndt and Goldstein, 1989; Kay and Kay, 1991; Jull and Kelemen, 2001; Escrig et al., 2004; Gao et al., 2004;

Elkins-Tanton, 2005; Lustrino, 2005; Anderson, 2006). This is due to the unique chemical and physical properties of eclogite formed by high to ultrahigh pressure metamorphism of basaltic rocks. Its density is higher than that of peridotite by 0.2–0.4 g cm<sup>-3</sup> (Rudnick and Fountain, 1995; Jull and Kelemen, 2001; Levander et al., 2006; Anderson, 2006), and because of this density contrast, eclogite formed at the base of thickened continental crust can be recycled into the mantle (Arndt and Goldstein, 1989; Kay and Kay, 1991; Jull and Kelemen, 2001; Gao et al., 2004). Eclogites have lower melting temperatures than mantle peridotites (Yaxley and Green, 1998; Rapp et al., 1999; Yaxley, 2000; Kogiso et al., 2003; Sobolev et al., 2005, 2007), and as foundered, silica-saturated eclogites heat up, they will produce silicic melts (tonalite to

\* Corresponding author. State Key Laboratory of Geological Processes and Mineral Resources, China University of Geosciences, Wuhan 430074, China. Tel.: +86 27 67884940; fax: +86 27 67885096.

E-mail address: [sgao@263.net](mailto:sgao@263.net) (S. Gao).

trondhjemite) that may react extensively with overlying mantle peridotite. Such reaction may produce an olivine-free pyroxenite, which, if subsequently melted, will generate basaltic melt (Kogiso et al., 2003; Sobolev et al., 2005; Herzberg, 2006; Sobolev et al., 2007).

Although recycling of eclogite in subducted oceanic lithosphere is a direct consequence of plate tectonics and its consequences for mantle composition have been extensively studied (e.g., Hawaii) (Hofmann and White, 1982; Sobolev et al., 2005; Herzberg, 2006; Sobolev et al., 2007), recycling of eclogite formed in deep continental lithosphere is more controversial and only a few studies have considered its effect on the composition of mantle-derived magmas (McKenzie and O'Nions, 1983; Arndt and Goldstein, 1989; Escrig et al., 2004; Elkins-Tanton, 2005; Lustrino, 2005; Anderson, 2006). Here we present petrographic and geochemical evidence that Mesozoic basalts and picrites from the North China craton derive from mantle that was modified by interaction with melts from foundered eclogite.

## 2. The North China craton

The North China craton (NCC) (Fig. 1) is one of the world's oldest Archean cratons, preserving crustal remnants as old as 3800 Ma (Liu

et al., 1992). The craton is divided into the Eastern Block, the Western Block and the intervening Trans-North China Orogen/Central Orogenic Belt based on age, lithological assemblage, tectonic evolution and  $P$ - $T$ - $t$  paths (Zhao et al., 2005) (Fig. 1). The NCC is also one of the world's most unusual cratons, as the eastern block was reactivated in the Mesozoic. We focus here on the history of the Eastern Block, which is where the lavas under investigation erupted during the Mesozoic.

The basement of the Eastern Block consists primarily of Early to Late Archean high- and low-grade TTG gneisses and 2500 Ma syntectonic granitoids, with locally preserved Early to Late Archean (3800–3000 Ma) granitic gneisses and supracrustal rocks (Liu et al., 1992; Zheng et al., 2004). This portion of the craton had a cold and thick lithosphere, typical of other Archean cratons, at least through the Ordovician, when kimberlites erupted that carried diamonds and refractory garnet peridotites (Menziés et al., 1993; Griffin et al., 1998), the latter of which have Archean Os model ages (Gao et al., 2002; Wu et al., 2006; Zhang et al., 2008).

Reactivation of the craton began in the Early Mesozoic, with uplift and the onset of magmatism, followed by basin development. The magmatism peaked volumetrically in the Late Cretaceous (120–132 Ma) (Wu et al., 2005). This early, compositionally diverse magmatism was

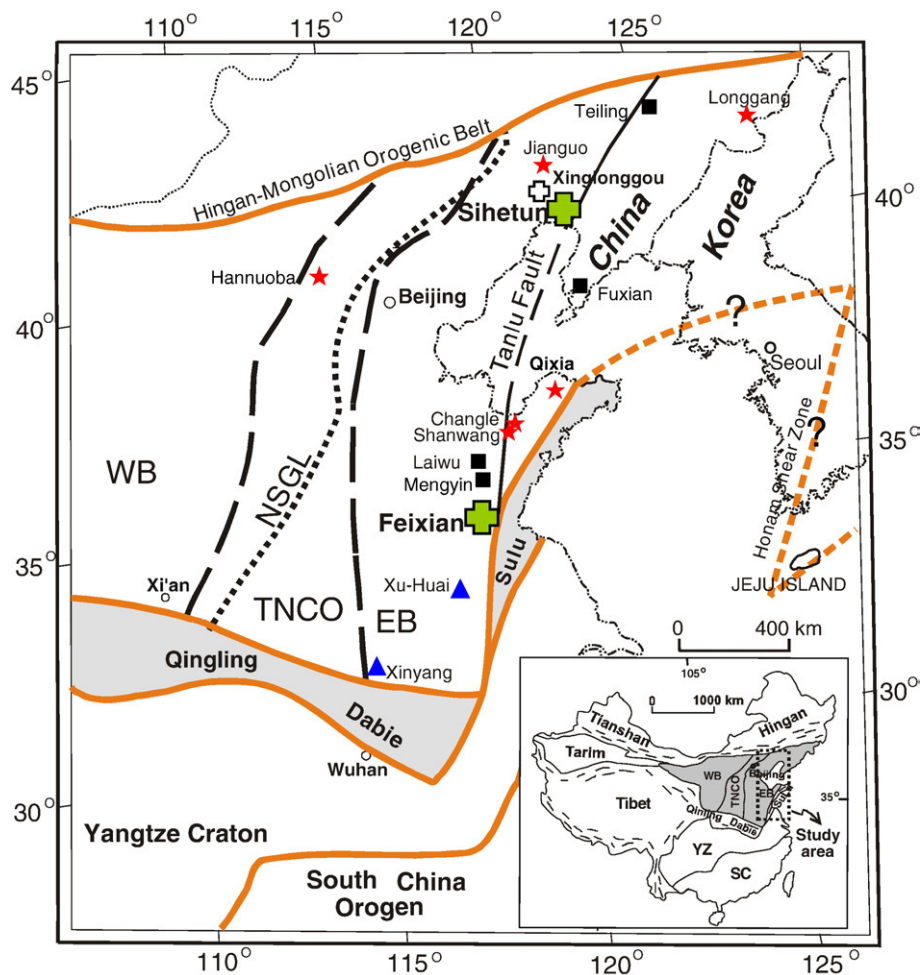


**Fig. 1.** Geologic sketch map of the North China craton (shaded on inset). The two suites of Early Cretaceous lavas under investigation (large filled crosses) are from Sihetun, in western Liaoning, and Feixian, in western Shandong. WB, TNCO and EB denote three-fold division of the North China craton into the Western Block, Trans-North China Orogen and Eastern Block, respectively (Zhao et al., 2005). NSGL indicates the North–South Gravity Lineament (Griffin et al., 1998). Also shown are locations of the Early Mesozoic high-Mg Xinglonggou intermediate–felsic lavas (open cross) (Gao et al., 2004), Archean peridotite xenoliths (squares) from Ordovician kimberlites [Teiling (Wu et al., 2006), Fuxian (Gao et al., 2002; Zhang et al., 2008), Menyin (Gao et al., 2002; Zhang et al., 2008)] and ~130 Ma high-Mg diorite (Laiwu) (Chen and Zhou, 2006; Xu et al., 2008) and younger peridotite xenoliths (stars) (Gao et al., 2002; Wu et al., 2003; Zheng et al., 2006) from Late Mesozoic (102–106 Ma, Jianguo, Zhu et al., 2004) or Cenozoic (Longgang, Qixia, Shangwang, Chengle, and Hannuoba) alkali basalts. Triangles designate granulite, pyroxenite and eclogite xenolith localities from Jurassic diatremes at Xinyang (Zheng et al., 2004) and 130–132 Ma high-Mg dioritic–monzodioritic porphyries at Xu-Huai (Xu et al., 2006). Inset shows major tectonic divisions of China, where the North China craton is shaded and YZ and SC denote the Yangtze craton and South China Orogen, respectively. The extension of the border between the North China craton and the Yangtze craton into Korea is based on Lee and Walker (2006).

followed by Cenozoic intraplate basaltic volcanism. Cenozoic basalts in the Eastern Block carry mantle xenoliths that equilibrated to a high geotherm (Xu, 2001; Zheng et al., 2006), have a relatively fertile bulk composition (Menzies et al., 1993; Griffin et al., 1998; Rudnick et al., 2004) and Os isotopic compositions similar to the modern convective mantle (Gao et al., 2002; Wu et al., 2003, 2006). Today, the Eastern Block of the NCC is characterized by high surface heat flow, slow seismic wave speeds in the lower crust and the upper mantle, unusually evolved lower and bulk crust compositions, thin lithosphere and strong seismicity (Gao et al., 1998a,b; Chen et al., 2006). In effect, the eastern block of the NCC is no longer a craton.

The above observations have been used to suggest that ancient, cratonic mantle lithosphere, similar to that present beneath the Kaapvaal, Siberian and other Archean cratons, was removed from the base of the Eastern Block of the NCC during the Mesozoic, and was replaced by younger, less refractory lithospheric mantle. Whether the replacement was caused by foundering, stretching or thermal/chemical erosion of the deep lithosphere due to upwelling asthenosphere is a matter of great debate (Xu, 2001; Gao et al., 2004; Wu et al., 2005; Menzies et al., 2007; Zhang et al., 2007; Huang et al., 2007).

Basalts and other magmatic rocks of Late Mesozoic age that are widespread in the eastern NCC (Wu et al., 2005) provide a window into the evolution of the craton during the critical period of lithospheric thinning. In particular, high-Mg andesites from the Xinglonggou locality in western Liaoning have distinctive petrographic and chemical features that suggest their origin from foundered lower crust of the NCC (Gao et al., 2004). These include reversely zoned orthopyroxene phenocrysts (that document interaction with peridotite), very high Ni and Cr contents (up to 300 and 400 ppm, respectively), ancient inherited zircons (with an age distribution similar to that of the NCC crust), as well as evolved initial Nd and Sr isotopic compositions ( $\epsilon_{\text{Nd}} = -3$  to  $+2$ ,  $^{87}\text{Sr}/^{86}\text{Sr} = 0.7057$  to  $0.7069$ ). Although these lavas have features similar to inferred slab melts (strongly fractionated REE, high Sr and high Mg#) they do not have the isotopic characteristics of such melts, which would be similar to MORB. Moreover, they cannot be slab melts that assimilated large quantities of NCC crust, as it would be impossible to preserve the very high Ni and Cr under such a scenario. The high Ni and Cr contents likewise rule out an origin through magma mixing between mantle-derived basalt and crustally-derived tonalite. Rather, these lavas were interpreted to have formed as melts derived from foundered NCC lower crust that interacted with mantle peridotite as they ascended (Gao et al., 2004). If this interpretation is correct, it implies that density foundering initiated in the Early Mesozoic beneath this portion of the NCC. It remains unclear how extensive this foundering may have been, its duration in time, and whether the foundering occurred as a single event or as diachronous events throughout the eastern block of the NCC.

Here we focus on Early Cretaceous alkaline picrites and high-magnesium basalts from two localities in the Eastern Block of the NCC, where the removal of lithospheric mantle and lower crust is most prominent.

### 3. Samples

Two suites of Early Cretaceous mafic magmas are investigated here: the Sihetun high-Mg basalts, which erupted in western Liaoning Province, and the Feixian alkaline picrites, which erupted in western Shandong Province (Fig. 1). We describe each suite, in turn.

The Sihetun basalts belong to the Yixian Formation and occur in the type section at Sihetun, 50 km southeast of the Xinglonggou lavas (Gao et al., 2004) (Fig. 1). This section consists of sandstone/conglomerates at the base, which are immediately overlain by high-Mg basalt (Table 1; Table S1). The middle and upper units consist of interlayered, thick, high-Mg andesites (Mg# = 55–67) (Wang et al., 2006), tuff and lacustrine sediments, the top of which contains feathered dinosaurs and is dated at 122 to 125 Ma (Zhou et al., 2003). The basal high-Mg basalt has a whole rock Ar–Ar age of 124–125 Ma (Fig. S1). This age is indistinguishable

from the age of the upper unit and suggests that the Sihetun high-Mg basalts formed within a few million years. The samples investigated here come from a  $\sim 1500$  m<sup>2</sup> exposure. The Sihetun high-Mg basalts are generally fresh and contain olivine and clinopyroxene phenocrysts. The olivines are euhedral and range in size up to  $5 \times 3$  mm, and are typically altered along grain boundaries and partings. The fine-grained matrix consists of plagioclase, pyroxene and opaque minerals.

Alkaline picrites from western Shandong (Table 1; Table S1) occur only sporadically near Feixian due to cover by Quaternary sediments and farmland (Fig. 1). They have a K–Ar age of  $119 \pm 2.3$  Ma (Pei et al., 2004). Like the western Liaoning locality, high-Mg andesite, dacite and their low-Mg counterparts are widespread in Shandong and are younger [98–106 Ma (Ling et al., 2006)] than the mafic magmas. The samples investigated here come from a small  $\sim 600$  m<sup>2</sup> outcrop. These picrites are very fresh and contain olivine, clinopyroxene and rare orthopyroxene phenocrysts, altered plagioclase and very rare quartz. Unlike the Sihetun olivine phenocrysts, the Feixian olivines are anhedral and much smaller (generally less than 1 mm) and show kink bands (Pei et al., 2004).

### 4. Analytical methods

Major element compositions of minerals were analyzed on a JEOL Superprobe JXA 8100 at the Department of Geology, Peking University, China. Trace element compositions of olivines and clinopyroxenes were analyzed using an excimer laser ablation inductively coupled plasma mass spectrometer (LA-ICP-MS) at the State Key Laboratory of Geological Processes and Mineral Resources, China University of Geosciences. Major and trace element compositions of whole rocks were measured by XRF and ICP-MS, respectively, at the State Key Laboratory of Continental Dynamics, Northwest University, China. Sr and Nd isotopic ratios were analyzed using a MC-ICP-MS also at the State Key Laboratory of Continental Dynamics, Northwest University, China. Rhenium–Os isotopic analyses of bulk samples and four chromite separates were carried out at the University of Maryland.

Full details of analytical methods are provided in Supplementary online materials.

### 5. Results

#### 5.1. Sihetun basalts

Euhedral olivine phenocrysts in the Sihetun basalts are magnesian ( $\text{Fo}_{88}$  to  $\text{Fo}_{92}$ ) and have relatively high CaO contents ( $>0.1$  wt.%) (Fig. 2). Their Ni contents are highly variable (0.2 to 0.6 wt.%), and range to compositions that are distinctly more Ni-rich than typical olivine phenocrysts (Fig. 3). In this respect they resemble olivines from Hawaiian basalts that are interpreted to derive from pyroxenitic sources (Sobolev et al., 2005, 2007). Two of the analyzed olivines have low CaO (0.06–0.08 wt.%) and  $\text{Fo}_{91-92}$  (Table S3).

Two populations of clinopyroxene phenocrysts are present in the basalts. The predominant population is unzoned with relatively high Mg# (84.6 to 89.1) and low jadeite (Jd) component (1.3–4.3 mol%). The second type of clinopyroxene is rare and shows reverse zoning. These have cores with lower Mg# and higher Jd component (1.8–8.8 mol%) compared to their rims (1.2–4.2 mol%), the latter of which are similar to the dominant clinopyroxene composition (Table S4). Complex oscillatory zoning patterns are also present and can be seen to overgrow the reversely zoned clinopyroxenes.

Euhedral chromites occur in olivine phenocrysts. Their Cr#s range from 54 to 67 with an average of 62 (Table S6). Such values are similar to those of chromites in Hawaiian lavas (Barnes and Roeder, 2001).

The Sihetun basalts have low CaO (7.2–8.3 wt.%) and high MgO contents (10.2 to 12.3 wt.%), Mg # (70–74) and Ni and Cr contents (up to 360 and 1100 ppm, respectively) (Table 1, Table S1). Trace element ratios of these basalts are distinctive, with  $100\text{Mn}/\text{Fe}$  (1.62–1.84) and  $\text{Ni}/\text{MgO}$  (18 to 29) slightly lower than values of typical peridotite-

**Table 1**  
Geochemical and isotopic compositions of selected Cretaceous basalts and mineral separates

	Sihetun high-Mg basalt										
	SHT-16	SHT-19	SHT-21	SHT-28	SHT-31	SHT-31	SHT-31	SHT-31	SHT33	SHT-33	SHT-36
	WR	WR	WR	WR	WR	Chr	Chr (dup)	Ol	WR	Chr	WR
Fo*	89.82	91.21	91.07	91.06	90.09						91.05
SiO <sub>2</sub>	49.90	49.81	49.41	50.19	50.52				51.53		49.77
TiO <sub>2</sub>	0.86	0.84	0.84	0.83	0.87				0.81		0.88
Al <sub>2</sub> O <sub>3</sub>	12.60	12.99	12.67	12.78	12.85				13.39		12.55
TFeO	7.57	7.68	7.64	7.68	7.53				7.18		7.81
MgO	12.29	11.03	11.05	10.86	11.51				9.72		10.77
CaO	7.30	7.83	8.08	8.14	7.32				7.53		8.47
Na <sub>2</sub> O	2.69	2.52	2.48	2.58	3.01				2.72		2.48
K <sub>2</sub> O	2.30	2.44	2.35	2.39	2.35				2.56		2.39
Mg#	74.3	71.9	72.1	71.6	73.1				70.7		71.1
Cr	1107	903	880	936	1062				822		1059
Ni	357	226	259	232	326				193		218
Sr	684	772	778	809	696				752		907
Y	20	23	23	23	20				22		22
La	54	61	58	58	51				56		57
Yb	1.61	1.64	1.42	1.59	1.56				1.55		1.64
Lu	0.23	0.24	0.21	0.23	0.23				0.22		0.24
Hf	3.57	3.65	3.44	3.58	3.79				3.72		3.79
Th	7.00	7.81	7.28	7.37	6.90				8.06		7.22
U	1.32	1.29	1.45	1.52	1.39				1.45		1.57
100Mn/Fe	1.73	1.66	1.71	1.62	1.84				1.65		1.71
Sr/Y	34	34	34	35	35				34		41
La <sub>N</sub> /Yb <sub>N</sub>	22.5	25.0	27.8	24.5	22.0				24.3		23.4
Eu/Eu*	0.95	0.95	0.97	0.97	0.95				0.95		0.95
Th/U	5.32	6.07	5.02	4.86	4.96				5.56		4.60
Ni/MgO	29	21	23	21	28				20		20
Lu/Hf	0.064	0.066	0.061	0.064	0.061				0.060		0.063
<sup>143</sup> Nd/ <sup>144</sup> Nd	0.512461	0.512445	0.512484	0.512490	0.512459						0.512457
2σ	5	3	4	5	4						2
ε <sub>Nd</sub> (125 Ma)	-2.10	-2.44	-1.73	-1.58	-2.16						-2.23
<sup>86</sup> Sr/ <sup>87</sup> Sr	0.706710	0.706613	0.706614	0.706593	0.706591						0.707035
2σ	14	18	10	15	12						17
<sup>86</sup> Sr/ <sup>87</sup> Sr (125 Ma)	0.706274	0.706227	0.706235	0.706224	0.706155						0.706712
Re (ppb)	0.048	0.039	0.098	0.067	0.070	0.036	0.221	0.002	0.113	0.059	0.065
Os (ppb)	0.721	0.106	0.604	0.208	0.145	38.86	23.61	0.222	0.071	18.18	0.145
<sup>187</sup> Os/ <sup>188</sup> Os	0.1650	0.2328	0.1920	0.1789	0.2075	0.1477	0.1619	0.2182	0.2388	0.1546	0.2059
2σ	2	3	2	3	3	1	2	7	4	3	3
<sup>187</sup> Re/ <sup>188</sup> Os	0.3226	1.7916	0.7918	1.5703	2.3448	0.0044	0.046	0.0452	7.769	0.016	2.1928
<sup>187</sup> Os/ <sup>188</sup> Os (125 Ma)	0.1643	0.2291	0.1904	0.1756	0.2026	0.1477	0.1615	0.2181	0.2227	0.1545	0.2013
γ <sub>Os</sub> (125 Mα)	30(5)	82(8)	51(5)	39(4)	61(11)	17(3)	28(3)	73(6)	77(4)	23(3)	60(9)
	Feixian alkaline picrite										
	SFX13	SFX19	SFX27	SFX28	SFX30	SFX57Chr	FX2-88	FX2-88Chr	FX2-90		
	WR	WR	WR	WR	WR	Chr	WR	Chr	WR		
Fo*	92.40	91.00		92.00	91.40		92.10				92.00
SiO <sub>2</sub>	48.61	48.68	49.18	49.47	48.91		48.29				48.29
TiO <sub>2</sub>	1.10	1.10	1.07	1.07	1.08		1.08				1.09
Al <sub>2</sub> O <sub>3</sub>	11.77	11.96	11.92	11.86	11.71		11.45				11.50
TFeO	7.97	7.98	7.88	7.87	8.04		8.10				8.09
MgO	13.61	13.42	13.02	13.06	13.60		14.57				14.26
CaO	8.78	8.79	8.74	8.76	8.84		8.75				8.82
Na <sub>2</sub> O	1.93	2.23	2.18	2.19	2.43		2.45				2.44
K <sub>2</sub> O	2.62	2.62	2.72	2.53	2.08		2.01				1.97
Mg#	75.3	75.0	74.5	74.7	75.1		76.2				75.9
Cr	737	741	724	736	788		863				839
Ni	456	453	424	426	469		519				497
Sr	1484	1493	1551	1511	1468		1437				1436
Y	29	38	24	23	23		25				28
La	100	102	104	101	95		132				133
Yb	1.64	1.77	1.73	1.64	1.59		1.79				1.78
Lu	0.22	0.23	0.23	0.21	0.21		0.25				0.25
Hf	4.63	4.86	4.77	4.63	4.43		5.27				5.24
Th	10.7	10.7	11.2	11.2	10.8		11.2				10.8
U	1.71	1.72	1.79	1.75	1.68		1.68				1.67
100Mn/Fe	1.58	1.58	1.59	1.59	1.58		1.58				1.58
Sr/Y	51	39	64	66	64		57				51
La <sub>N</sub> /Yb <sub>N</sub>	41.2	39.1	40.6	41.3	40.4		50.1				50.6
Eu/Eu*	0.97	0.96	0.97	0.96	0.96		0.98				0.98
Th/U	6.26	6.21	6.22	6.39	6.43		6.64				6.48
Ni/MgO	34	34	33	33	34		36				35

Table 1 (continued)

	Feixian alkaline picrite								
	SFX13	SFX19	SFX27	SFX28	SFX30	SFX57Chr	FX2-88	FX2-88Chr	FX2-90
	WR	WR	WR	WR	WR	Chr	WR	Chr	WR
Lu/Hf	0.047	0.047	0.048	0.045	0.047		0.047		0.048
<sup>143</sup> Nd/ <sup>144</sup> Nd	0.511884	0.511885	0.511882	0.511875	0.511870		0.511885		
2σ	8	6	6	6	7		7		
ε <sub>Nd</sub> (119 Ma)	-13.1	-13.1	-13.17	-13.3	-13.4		-13.1		
<sup>86</sup> Sr/ <sup>87</sup> Sr	0.710089	0.710023	0.710017	0.709918	0.709906		0.710024		
2σ	10	14	16	15	18		15		
<sup>86</sup> Sr/ <sup>87</sup> Sr (119 Ma)	0.709903	0.709858	0.709843	0.709813	0.709767		0.709872		
Re (ppb)	0.274	0.236	0.237	0.229	0.262	2.5	0.199	7.5	0.225
Os (ppb)	0.189	0.217	0.123	0.146	0.124	5.128	0.179	0.704	0.107
<sup>187</sup> Os/ <sup>188</sup> Os	0.2533	0.2195	0.2454	0.2496	0.3165	0.1443	0.2208	0.186	0.2351
2σ	4	4	5	5	7	12	5	7	5
<sup>187</sup> Re/ <sup>188</sup> Os	7.099	5.30	9.43	7.65	10.4	2.3	5.432	37	10.2
<sup>187</sup> Os/ <sup>188</sup> Os (119 Ma)	0.239	0.209	0.227	0.234	0.296	0.140	0.210	0.112	0.215
γ <sub>Os</sub> (119 Mα)	90(2)	66(4)	80(5)	86(5)	134(5)	11(4)	66(2)	-11(20)	70(4)

Major oxides are reported in weight percent (wt.%), Re and Os in parts per billion (ppb) and other trace elements in parts per million (ppm). TFeO, total iron as FeO; Mg#, molar  $100 \times \text{Mg}/(\text{Mg} + \text{Fe})$ .  $\text{Eu}/\text{Eu}^* = \text{Eu}_N/(\text{Sm}_N + \text{Gd}_N)^{1/2}$ , where subscript  $N$  denotes chondrite normalization. WR indicates whole rock. Chr and Ol denote chromite and olivine separates, respectively. dup represents duplicate analysis. \*Average forsterite content ( $\text{Fo} = 100 \times \text{Mg}/(\text{Mg} + \text{Fe})$ , where Mg and Fe represent molar proportions) of olivines determined by electron microscope. Complete geochemical and Sr–Nd–Pb isotopic compositions for the basalts are given in Table S1 in Supplementary online materials.  $\gamma_{\text{Os}}$  is calculated as per Shirey and Walker (1998). Uncertainties in  $\gamma_{\text{Os}}$  as last significant figures are shown in parentheses.

derived basalts ( $100\text{Mn}/\text{Fe} = 1.90$ ,  $\text{Ni}/\text{MgO} = 34$ ; Sobolev et al., 2007). The Sihetun basalts also have high Sr/Y (34 to 43) and  $\text{La}_N/\text{Yb}_N$  ratios (22 to 28), which are similar to those of Archean tonalite–trondhjemite–granodiorites and modern adakites (Martin et al., 2005).

The basalts are isotopically evolved, with limited variation in initial  $\epsilon_{\text{Nd}}$  (-1.6 to -2.4) and  $^{87}\text{Sr}/^{86}\text{Sr}$  (0.7061 to 0.7067) (Table 1). The Os isotope systematics of the basalts are more complex. Whole rock samples of the basalts have Os concentrations ranging from 0.071 to 0.72 ppb (Table 1). Initial  $\gamma_{\text{Os}}$  (125 Ma) values are variable and range from +30 to +82. Chromites separated from magmatic rocks are often examined for Re–Os isotopic systematics because they tend to concentrate Os and exclude Re, making them reliable recorders of initial magmatic  $^{187}\text{Os}/^{188}\text{Os}$  (Walker et al., 2002). Chromite separates from two Sihetun basalts (SHT-31 and SHT-33) are typical of magmatic chromites worldwide. They have high Os (>10 ppb) and low Re (<0.3 ppb) concentrations, and very low Re/Os. Because of the very low Re/Os, age corrections are negligible for the separates, which are less radiogenic than the whole rocks. Duplicate analyses of the chromite separates from SHT-31 (different aliquots of powder) give different  $\gamma_{\text{Os}}$  (125 Ma) values of +17 and +28, which vary substantially beyond analytical uncertainties (about  $\pm 0.3$   $\gamma_{\text{Os}}$  units). Chromite SHT-33chr has an intermediate  $\gamma_{\text{Os}}$  (125 Ma) value of +23. Furthermore, the chromite compositions for SHT-31 and SHT-33 diverge considerably from those of their bulk samples [ $\gamma_{\text{Os}}$  (125 Ma) = +61 and +77, respectively], and from olivine separated from SHT-31, which has a more radiogenic initial ratio than the bulk sample [ $\gamma_{\text{Os}}$  (125 Ma) = +73]. Thus, the minerals were not in isotopic equilibrium with the bulk sample at the time of eruption, nor were individual crystals of one mineral (e.g., chromite) uniform in isotopic composition.

## 5.2. Feixian picrites

There are two populations of olivines in the Feixian picrites. One population has a euhedral morphology and is relatively magnesian ( $\text{Fo}_{84}$  to  $\text{Fo}_{91}$ ) with high CaO contents (>0.1 wt.%) (Fig. 2). Compared to the olivine phenocrysts in the Sihetun basalts, these olivines tend to have lower Fo and Ni contents. Most of them have similar compositions to Hawaiian olivine phenocrysts, which overlap the field of common olivine phenocrysts; a few have distinctly higher Ni than common olivine phenocrysts (Fig. 3). The second population is anhedral and has high Fo (92–93), low Ca (<0.1 wt.%) cores surrounded by rims that have compositions similar to the first population (Fig. 3; Fig. S2).

Like the Sihetun basalts, two populations of clinopyroxenes are also present in the Feixian picrites (unzoned augites vs. reversely

zoned clinopyroxenes with high Jd cores, Fig. 4). However, the zoned clinopyroxenes are far more abundant in the Feixian picrites compared to the Sihetun basalts (Table S5) and some contain ilmenite exsolution lamellae in their cores (Fig. 5a and b), a feature not observed in the clinopyroxenes from the Sihetun basalts.

Chromites in the Feixian picrites also occur in olivine phenocrysts and are euhedral to anhedral. Chromites within the high Mg olivines have high Cr# [62 to 69, with an average of 65 (Table S6)], which suggests their derivation from a refractory source (Pearson et al., 2003).

The Feixian picrites are alkaline (4.3–4.9%  $\text{Na}_2\text{O} + \text{K}_2\text{O}$ ) with high Mg# (75–76). Compared with the Sihetun basalts, these picrites have slightly higher CaO (~8.5 wt.%), higher Ni (401–519 ppm) and Cr (590–866 ppm) contents, higher Ni/MgO (32 to 36), lower  $100\text{Mn}/\text{Fe}$  (~1.55) and higher Sr/Y (40 to 70) and  $\text{La}_N/\text{Yb}_N$  (39–51) (Table 1, Table S1).

The Sr and Nd isotopic compositions of the picrites are more evolved and more homogeneous than the Sihetun basalts. Initial  $\epsilon_{\text{Nd}}$  values do not vary beyond analytical uncertainty, averaging -13. Initial  $^{87}\text{Sr}/^{86}\text{Sr}$  is slightly more variable, ranging only from 0.70977 to 0.70990 (Table 1 and Table S1). The Os concentrations in seven whole rock samples of the picrites range from 0.11 to 0.22 ppb. Initial  $\gamma_{\text{Os}}$  (119 Ma) values for the whole rock samples are variable and high, ranging from +66 to +134, so like the Sihetun basalts, the bulk samples of the picrites are isotopically heterogeneous.

Two chromite separates are enriched in Os relative to bulk samples, but, unlike Sihetun chromites, have suprachondritic Re/Os. Furthermore, only limited chromite could be separated from these rocks, so Re blank corrections are proportionally very large from these samples. The relatively high Re/Os, combined with uncertainties in Re lead to large uncertainties in age corrected initial ratios. Despite the large uncertainties, the two chromite separates from the picrites are resolvable much less radiogenic than the whole rock samples. Chromite separate SFX-57chr has a  $\gamma_{\text{Os}}$  (119 Ma) of  $+11 \pm 4$ ; FX2-88chr has a  $\gamma_{\text{Os}}$  (119 Ma) of  $-11 \pm 20$ . As with the Sihetun basalts, the chromites were not in isotopic equilibrium with the whole rocks at the time of eruption.

## 6. Discussion

### 6.1. Magmatic and xenocrystic olivines

The morphologies, structure and composition of olivines from both the Sihetun basalts and Feixian picrites provide important clues about their origins and the nature of the deep lithosphere during the Late Cretaceous. The euhedral, high CaO (>0.10%), lower Fo olivines (< $\text{Fo}_{92}$ )

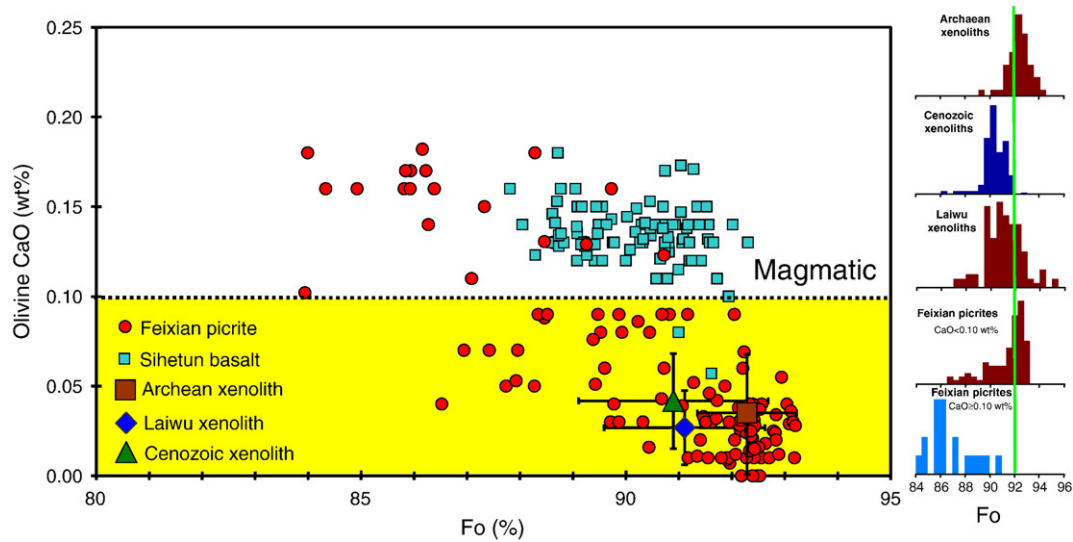


**Fig. 2.** (Left) Fo (forsterite =  $100 \text{ Mg}/(\text{Mg} + \text{Fe})$ , where Mg and Fe represent molar proportions) versus wt.% CaO plot of olivine cores from Early Cretaceous Feixian alkaline picrites and Sihetun high-Mg basalts. Average compositions ( $\pm 1\sigma$ ) of olivines from NCC peridotite xenoliths are shown for comparison [large square: Archean peridotite xenoliths from Ordovician kimberlites; diamond: peridotite xenoliths from Early Cretaceous (~130 Ma) high-Mg diorite (Laiwu); triangle: lherzolite xenoliths from Cenozoic alkali basalts]. High Fo peridotites (Ordovician kimberlites and some Laiwu xenoliths) derive from Archean NCC lithosphere. Lower Fo peridotites (some Laiwu xenoliths and Cenozoic basalt xenoliths) represent younger lithospheric mantle formed after removal of the Archean mantle. Olivines from the Sihetun basalts have  $\text{CaO} \geq 0.10\%$ , characteristic of a magmatic origin (Thompson and Gibson, 2000) and  $\text{Fo}_{89-92}$  in the core. In contrast, those from the Feixian picrites show a range of  $\text{CaO} (< 0.01 \text{ to } 0.18\%)$ , indicating both phenocrystic and xenocrystic origins. (Right) Fo histograms show the systematic compositional differences in olivines from different sources. Olivines from the Feixian picrites, with  $\text{CaO} \geq 0.10\%$ , have  $\text{Fo} < 92$ , consistent with a magmatic origin, whereas those with  $\text{CaO} < 0.10\%$  have  $\text{Fo} > 92$ , consistent with a xenocrystic origin. See Supplementary online materials for data sources.

in both the Sihetun basalts and Feixian picrites are likely to be magmatic in origin (Thompson and Gibson, 2000). We will refer to these olivines henceforth as phenocrysts. Calculated Mg–Fe partition coefficients between the cores of the most forsteritic phenocrysts and whole rocks range from 0.30 to 0.33 (Table S7), consistent with experimental values ( $0.30 \pm 0.03$ ) (Roeder and Emslie, 1970). Thus, the high MgO contents of these lavas are not simply due to olivine accumulation, but rather reflect their origin as primary mantle melts.

In addition to the magmatic olivines, the Feixian picrites also contain anhedral, low CaO olivines (i.e.,  $< 0.10\%$ , Fig. S2) that have high  $\text{Fo}_{92-93}$

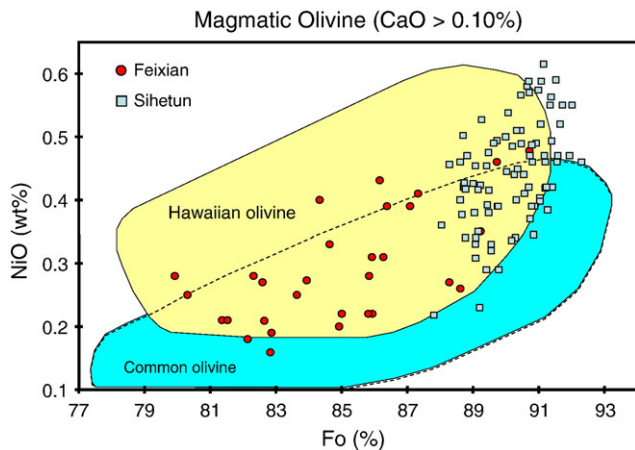


**Fig. 3.** Compositions of magmatic olivines ( $\text{CaO} > 0.10\%$ ) from Cretaceous basalts of the North China craton. The “common olivine” field outlines the compositional range for olivines from peridotites from mantle xenoliths, orogenic massifs and ophiolites, oceanic abyssal and mid-ocean-ridge basalts (Sobolev et al., 2005), while the Hawaiian olivine field denotes the range for olivine from Hawaiian basalts, which are interpreted to be derived from a hybridized pyroxenitic source formed by reaction of mantle peridotite with melts derived from recycled eclogitic oceanic crust (Sobolev et al., 2005). Olivine crystallized from pyroxenite-derived melt is Ni-rich, reflecting a paucity of olivine in the pyroxenite source (Sobolev et al., 2005, 2007). Magmatic olivines from both the Feixian picrites and Sihetun basalts are also Ni enriched. Note that most olivines in the Feixian picrites are xenocrystic ( $\text{CaO} < 0.10\%$ ) and are thus not shown.

cores (Table S3). They contain kink bands typical of mantle olivines (Pei et al., 2004), and are, thus, unlike forsterite-rich, low Ca, high Ni olivines interpreted to be of magmatic origin (Kamenetsky et al., 2006). The latter are euhedral to subhedral or ellipsoidal in shape, lack kink bands and have highly variable CaO contents ( $< 0.10\%$  to  $0.30\%$ ) at  $\text{Fo}_{91-94}$ . The Feixian high Fo olivines are distinctly more magnesian than olivines from lherzolite xenoliths entrained in Cenozoic alkali basalts in eastern China and are compositionally similar to olivines in garnet peridotite xenoliths from Ordovician kimberlites that sampled the Archean NCC mantle (Fig. 2; Table S3). These crystals are, thus, likely to be mantle xenocrysts and document the presence of Archean mantle lithosphere in the Early Cretaceous beneath Shandong. In addition, some olivine xenocrysts have high CaO rims ( $> 0.1\%$ ) and  $\text{Fo} < 92$  that reflect later magmatic overgrowth (Fig. S2).

Olivine phenocrysts from the high-Mg basalts and a few from the picrites have compositions that range to unusually high Ni contents (Fig. 3). In this respect they are similar to olivines from Hawaiian basalts that have been interpreted to derive from hybridized eclogite–peridotite sources where olivine is consumed and Ni becomes incompatible (Sobolev et al., 2005, 2007) (Fig. 3). These olivine compositions may thus reflect a similar source for the Mesozoic lavas.

## 6.2. Reconstructing primary melt compositions

The primary melt compositions of the high-Mg basalts and alkaline picrites (Fig. 6) were calculated using the PRIMELT1 software of Herzberg et al. (2007) by addition of olivine to the samples until the composition reached the cotectic  $[\text{L} + \text{opx} + \text{cpx} + \text{gt}]$  or  $[\text{L} + \text{ol} + \text{cpx} + \text{gt}]$ .  $\text{Fe}^{2+}/\Sigma\text{Fe}$  is assumed to be 0.90 in samples before olivine addition (Herzberg, 2006). The Fe–Mg exchange coefficient (Kd) for olivine–L and Fo for olivine are calculated using the method of Toplis (2005) at 1 atm. The primary melts for both lavas fall along the 3–4 GPa cotectics, implying relatively high derivation pressures. In addition, the primary melts have low CaO (6.1 to 8.0 wt.%) and FeO (6.9 to 8.1 wt.%) (see Table S8), both of which are consistent with derivation from a pyroxenitic, rather than peridotitic source at these pressures (see Section 6.4).

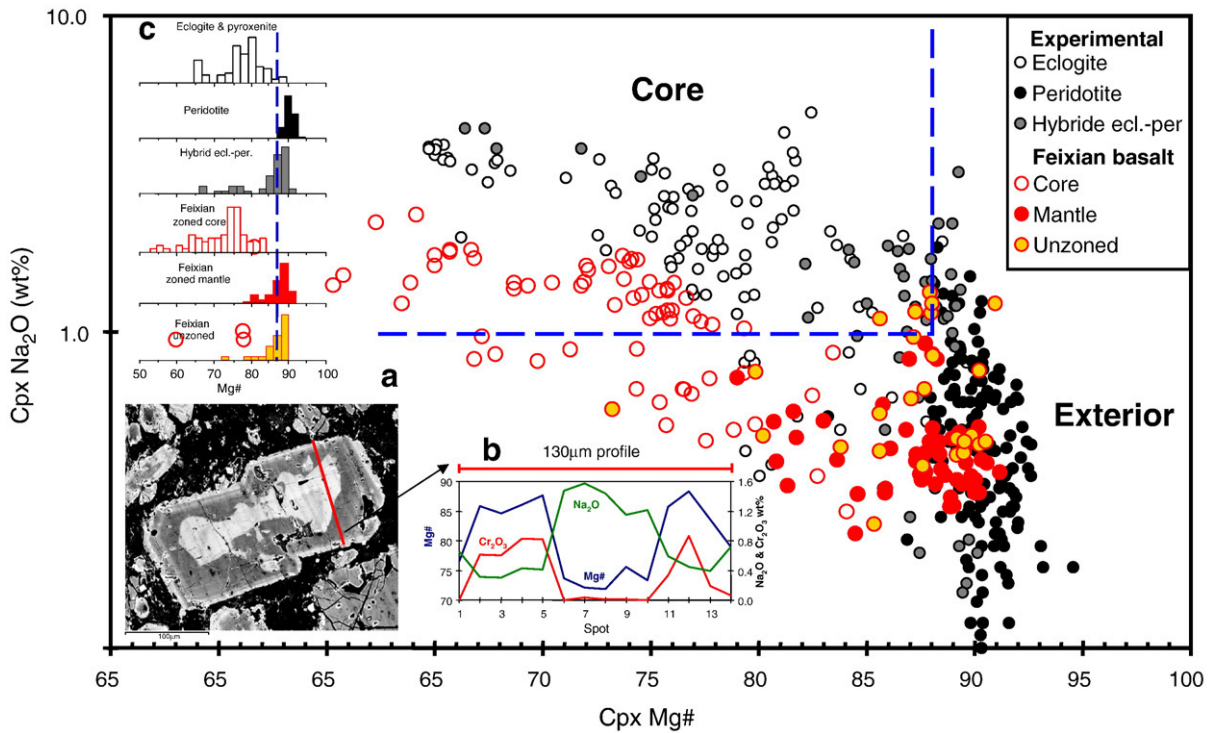


**Fig. 4.** Core-exterior compositions of reversely zoned clinopyroxene phenocrysts from the Feixian alkaline picrites. (a) backscattered electron image (BSE) and (b) compositional profile of a euhehedral clinopyroxene phenocryst along [010] plane from sample SFX19. The dark areas are Mg-rich and the light areas are Fe-rich. In contrast to the Fe- and Na-enriched core, the exterior shows markedly higher Mg (thus higher Mg#) and Cr contents. The sharp and irregular boundary between the core and mantle indicates that the mantle is a later overgrowth by chemical reaction, with little diffusive exchange between the two regions. In contrast, the compositional variation at the edge of the crystal is regular, and likely reflects shallow-level differentiation. The main Mg# versus Na<sub>2</sub>O plot and (c) Mg# histogram compare experimental clinopyroxenes in equilibrium with melts derived from eclogite (including garnet pyroxenite), peridotite and hybrid eclogite (ecl.)-peridotite (per.). Clinopyroxenes from eclogite-derived melt are characterized by Mg# < 87 and Na<sub>2</sub>O > 1.0%, as demarcated by the dash lines, whereas most of those from peridotite-derived melt, whether from anhydrous or hydrous melting, have higher Mg# and lower Na<sub>2</sub>O. Clinopyroxenes from hybrid eclogite–peridotite melt overlap the entire range of those from eclogite- and peridotite-derived melts. Although eclogite and clinopyroxenite with high Mg# [either in whole rocks, e.g. >81 (Kogiso and Hirschmann, 2001) or clinopyroxene ~91 (Skjerlie and Patino Douce, 2002)] may produce melts yielding clinopyroxene with Mg# similar to those from peridotite-derived melt, such high Mg#s are considerably higher than those found in common eclogites and their clinopyroxenes and also those of the Xu-Huai eclogites/garnet clinopyroxenites (Mg# < 75) and clinopyroxenes (Mg# < 85), which are considered a good approximation for the mafic lower crust of the North China craton (Gao et al., 2004; Xu et al., 2006). These experimental data are therefore not included in the comparison. The core and exterior compositions are consistent with crystallization of the clinopyroxenes from eclogite- and peridotite-derived melts, respectively, and agree with the compositional range of clinopyroxenes from hybrid, eclogite–peridotite-derived melt. See Supplementary online materials for data sources.

### 6.3. Evidence for a deep eclogite component in reversely zoned clinopyroxenes

The two suites of lavas contain reversely zoned clinopyroxene phenocrysts, which, like the olivines described above, provide important clues about the origin of these lavas. The irregular, resorbed cores of reversely zoned clinopyroxenes have low Mg# but high Na<sub>2</sub>O (2.35 wt.%, corresponding to 17.3 mol% Jd) and are surrounded by an exterior region with distinctly higher Mg, Cr and Ni but low Na<sub>2</sub>O (<0.95 wt.%, corresponding to <7.0 mol% Jd) (Fig. 4). These features are similar to those seen in reversely zoned orthopyroxenes from the Xinglonggou adakitic lavas, which were interpreted to reflect interaction of an eclogite-derived melt with mantle peridotite (Gao et al., 2004). The sharp and irregular boundary between the pyroxene core and mantle indicates that the latter formed as an overgrowth on resorbed crystals, with little diffusive exchange occurring between the two regions. The core and exterior compositions are consistent with crystallization from eclogite- and peridotite-derived melts, respectively (Fig. 4). The core-exterior compositions also overlap the large compositional range of clinopyroxene crystallized from melts derived from peridotite that has been variably hybridized by interaction with an eclogite-derived melt (Yaxley and Green, 1998) (Fig. 4).

Several compositional and petrographic features of the clinopyroxene cores suggest their crystallization at very high pressures (>2.5 GPa). The Na<sub>2</sub>O concentration and Jd component of magmatic clinopyroxenes are pressure-dependent ( $r=0.55$  to  $0.58$ , Fig. 5c), but

are temperature independent ( $r=-0.27$  to  $-0.29$ ) (Fig. 5d). The maximum Na<sub>2</sub>O of the cores (2.4 wt.%) (corresponding to 17.3 mol% Jd) and exteriors (0.92 wt.%) (corresponding to 6.5 mol% Jd) of the Feixian clinopyroxenes (Table S5), thus, reflect equilibration at pressures of  $\geq 2.5$  and  $\geq 1.5$  GPa, respectively. In addition, some cpx cores contain ilmenite exsolution lamellae, whereas the mantles are lamellae-free (Fig. 5a and b). Such lamellae have been described in clinopyroxenes from ultrahigh pressure eclogite and garnet pyroxenite, as well as peridotite xenoliths from kimberlite, and are interpreted to form upon decompression and /or cooling (Liou et al., 1998). These lines of evidence suggest that the clinopyroxene cores formed at a significantly greater depth than the exteriors.

Although reversely zoned phenocrysts are often attributed to mixing between a mantle-derived and crustal-derived melt at crustal depths, such an origin is unlikely for the Feixian clinopyroxenes. First, the evidence presented above shows that the cores of the phenocrysts, which, based on their low Mg# would represent the crustal component, must have formed at mantle pressures. Secondly, reversely zoned clinopyroxenes observed in high-Mg andesites that are interpreted as mixing products of mafic and felsic magmas at crustal depths (Guo et al., 2007; Streck et al., 2007) have systematically low Al<sub>2</sub>O<sub>3</sub> contents ( $\leq 3\%$ ). In contrast, the Feixian clinopyroxenes show variable and high Al<sub>2</sub>O<sub>3</sub> contents (up to 6.9% for the cores and 6.2% for the mantles) (Table S5), reflecting crystallization from an aluminous melt at mantle pressures (Streck et al., 2007 and references therein).

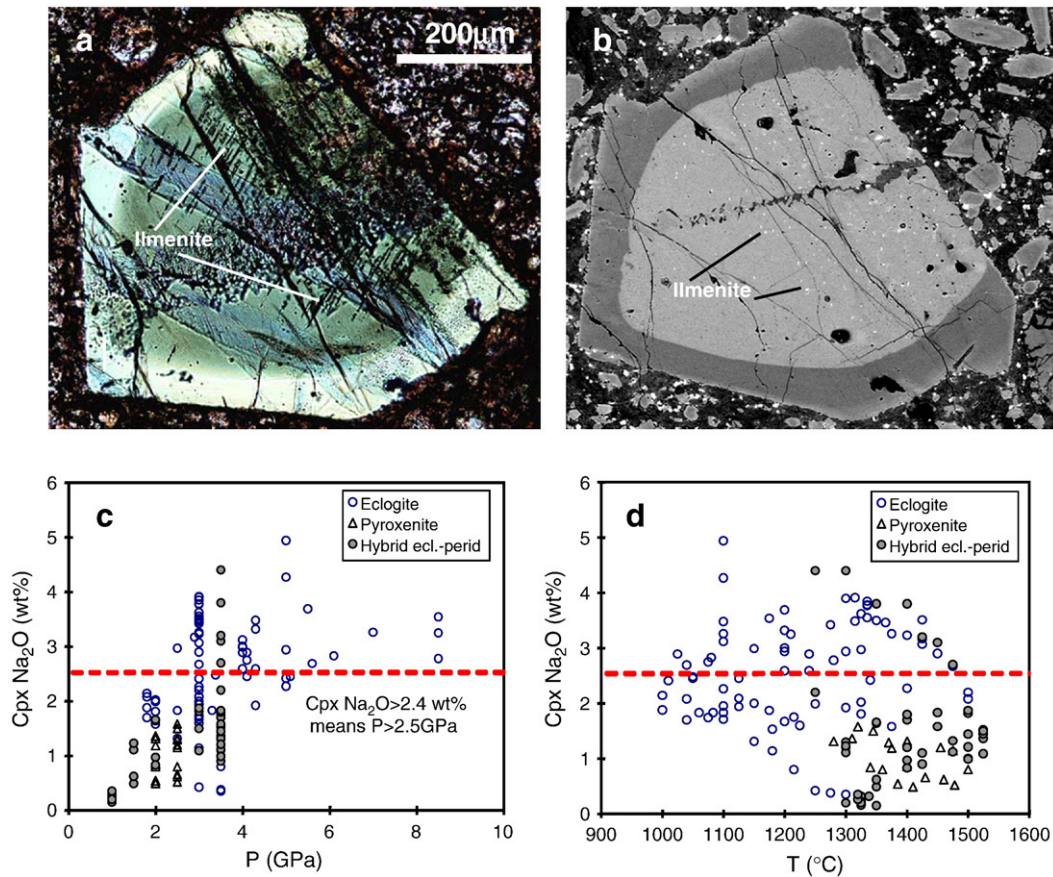


**Fig. 5.** (Upper) Exsolution lamellae of ilmenite in the core of one reversely zoned clinopyroxene phenocryst from Feixian alkaline picrite SFX28. (a) Photomicrograph under plane-polarized light. (b) Backscattered electron image. The low-Mg core corresponds to the green and light gray areas, while the high-Mg exterior to the light yellow and dark areas, in (a) and (b), respectively. Parallel black needles in (a), along the [010] crystallographic plane are ilmenite, as determined by electron microprobe analysis, while they appear as light dots in (b). The ilmenite lamellae are confined to the core of the crystal. (Lower)  $\text{Na}_2\text{O}$  content in experimental clinopyroxene in equilibrium with melt derived from eclogite, pyroxenite and hybrid eclogite (eccl.)–peridotite (per.) as a function of (c) pressure and (d) temperature. The  $\text{Na}_2\text{O}$  content of clinopyroxene depends upon pressure but not upon temperature, with correlation coefficient  $r=0.55$  and  $-0.27$ , respectively. The maximum  $\text{Na}_2\text{O}$  of the Feixian clinopyroxene cores (2.4 wt%) and exterior (0.92 wt%) (Table S5) reflect crystallization at pressures of  $\geq 2.5$  and  $\geq 1.5$  GPa, respectively. Calculated jadeite proportion of the clinopyroxene shows a similar correlation with pressure ( $r=0.58$ ). See Supplementary online materials for experimental data sources.

The zoned clinopyroxenes described here have similarities to the so-called green-cored clinopyroxenes found in alkaline basalts from the Massif Central, France, and elsewhere, which have relatively high Na cores (typically containing apatite inclusions) surrounded by lower Na rims (Pilet et al., 2002, 2005 and references therein). These green-cored clinopyroxenes were interpreted to have crystallized from asthenospheric melts that interacted with metasomatized lithospheric mantle. The latter imparted Nb- and Ta-depletion due to precipitation of rutile in metasomatic veins (Pilet et al., 2002, 2005). These Nb- and Ta-depleted melts imparted low Nb/Th to the cores of the cpx, but in all cases the rims of the cpx have high Nb/Th, consistent with crystallization from typical Nb-rich alkali basalts. Unlike the green-cored clinopyroxenes, the North China zoned clinopyroxene, in both core and exterior, show ubiquitous negative Nb–Ta anomalies (Table S2) and contain no apatite inclusions. Therefore, the green-cored clinopyroxenes found in alkaline basalts have a different origin from the cpx in the Mesozoic lavas from the North China craton.

#### 6.4. Geochemical characteristics of the source

##### 6.4.1. Incompatible trace elements

The trace element compositions of the clinopyroxene cores found in the Feixian picrites provide further constraints on their origin. Rare earth element compositions of melts in equilibrium with the clinopyroxene cores were calculated using experimentally determined clinopyroxene–tonalitic melt partition coefficients (Barth et al.,

2002a). These melts have fractionated rare earth element patterns, with no Eu anomalies, and high Sr/Y ratios, all features of eclogite-derived adakitic melts (Fig. 7)(Rapp et al., 1991; Hirschmann and Stolper, 1996; Rapp et al., 1999; Barth et al., 2002a; Gao et al., 2004; Martin et al., 2005; Sobolev et al., 2005; Xiong, 2006). Moreover, the picrites themselves have elevated  $\text{La}_N/\text{Yb}_N$  (39–51) and Th/U (6.2–6.8) and low Lu/Hf (0.046–0.049)(Table 1, Table S1). These features are unlikely to be due to crustal contamination, as the average continental crust has significantly lower  $\text{La}_N/\text{Yb}_N$  (8.2–11.7) and Th/U (3.8–6.0), and higher Lu/Hf (0.06–0.13) ratios (Rudnick and Gao, 2003).

##### 6.4.2. Major elements and compatible trace elements

The above trace element features are consistent with the derivation of the Feixian picrites from a peridotite that was hybridized by addition of adakitic melt derived from eclogite to form an olivine-poor, garnet-bearing pyroxenite source (Hirschmann and Stolper, 1996; Sobolev et al., 2005, 2007). Such a hybridized source is consistent with other geochemical features of these lavas. For example, the primary melts of the Feixian picrites appear to have formed along the L+Ol+Cpx+Gt cotectic at pressures between 3 and 4 GPa (Fig. 6a). In addition, the unusually low CaO contents of both the whole rocks (Table 1; Table S1) and reconstructed primary melts (7.5–8.0 wt.% CaO, Table S8) (Fig. 6b) are indicative of a pyroxenitic source. As shown by Herzberg (2006), primary melts from peridotite at pressures up to 7 GPa have an almost constant CaO content (10 wt.%), regardless of the degree of fertility of the peridotites being melted. The

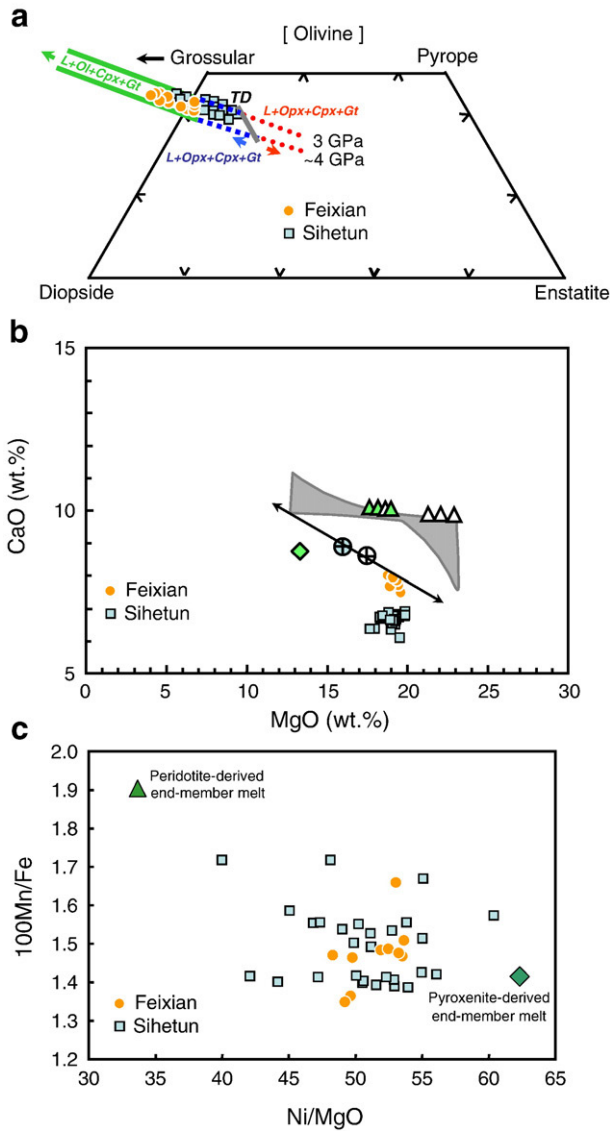


**Fig. 6.** Compositions of primary melts calculated for the Feixian alkaline picrites and Sihetun high-Mg basalts. (a) Mole% projection from or towards olivine into part of the pyroxene–garnet plane compared with cotectics at 3 and 4 GPa (Herzberg, 2006). Thick line labelled “TD” is the thermal divide between olivine-rich and SiO<sub>2</sub> rich sides of the composition space. Note that except for three Sihetun samples, which appear to have melted along the cotectic L+Ol+Cpx+Gt, the other Sihetun samples appear to have melted along the cotectic L+Opx+Cpx+Gt on the olivine-rich side. In contrast, all Feixian samples appear to have melted along the cotectic L+Ol+Cpx+Gt. (b) MgO versus CaO. Filled and open triangles indicate primary melts and solidus melts from peridotites (Herzberg, 2006; Sobolev et al., 2007), while filled diamond represents primary melt from pyroxenite (Sobolev et al., 2007). Shaded area denotes accumulated fractional melt compositions for a pressure range from 3 to 7 GPa (Herzberg, 2006). Filled and open circles with a cross indicate high- and low SiO<sub>2</sub> Hawaiian parental magmas (Herzberg, 2006). Arrows display the effects of olivine addition (right pointing) and subtraction (left pointing) (Herzberg, 2006). The Feixian and Sihetun primary melts are too low in CaO to be derived from normal mantle peridotites. Instead, they likely derive from pyroxenite sources. (c) Ni/MgO versus 100Mn/Fe ratios of primary melts compared to experimentally produced peridotite-(FeO=9.68 wt.%, MnO=0.185 wt.%, MgO=19.07 wt.%, Ni=642 ppm, 100Mn/Fe=1.90, Ni/MgO=34) and pyroxenite-derived (FeO=8.24 wt.%, MnO=0.117 wt.%, MgO=13.32 wt.%, Ni=830 ppm, 100Mn/Fe=1.42, MgO=62) end-member melts [Supplementary Table S2 of Sobolev et al. (2007)].

low CaO content of the primary melts of both the Feixian picrites and Sihetun basalts is similar to those derived from pyroxenites.

A pyroxenitic source is also consistent with the high Ni/MgO and low 100Mn/Fe observed in the two suites of lavas (Table 1; Table S1) and their reconstructed primary melts compared to peridotite-derived melt (Sobolev et al., 2007) (Fig. 6c). The fact that the Chinese

primary melts have Ni/MgO ratios lower than that calculated for pyroxenite-derived melt by Sobolev et al. (2007) may be due to the variable and lower Ni contents of their source pyroxenites [e.g., pyroxenite xenoliths entrained in the Mesozoic Laiwu diorite from the NCC (Fig. 1) have 380–600 ppm Ni; see below for discussion] compared to the relatively high Ni (1000 ppm) pyroxenite assumed by Sobolev et al. (2007).

#### 6.4.3. Sr, Nd and Os isotopes

Radiogenic isotopes can provide further insight into the source of the eclogite-derived melts and the nature of the original peridotites. However, before interpreting the isotopic compositions of the lavas in terms of their source region, the effect of crustal assimilation on these

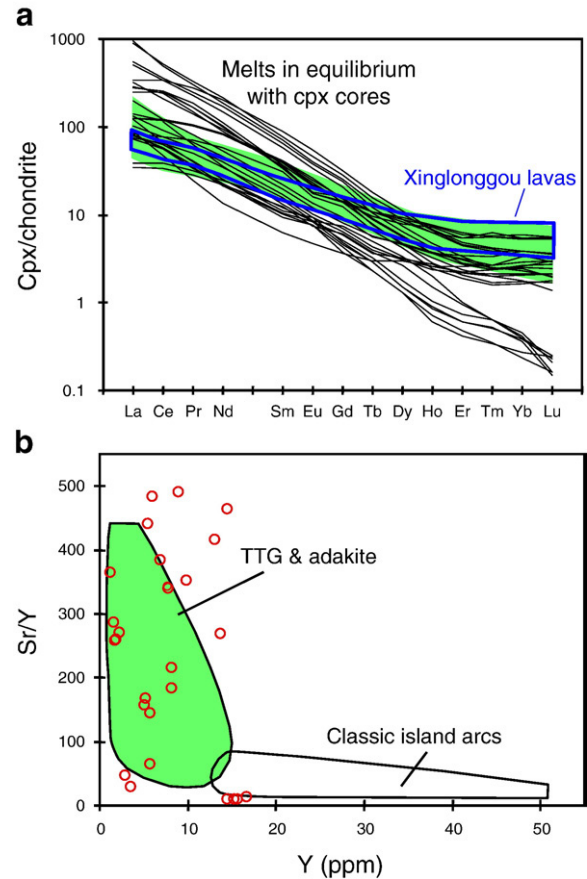


**Fig. 7.** Trace element compositions of melts calculated to be in equilibrium with cores of reversely zoned clinopyroxene phenocrysts from the Feixian picrites. Experimentally determined partition coefficients for clinopyroxene in equilibrium with eclogite-derived melt correlate with aluminium content of clinopyroxene (Pertermann and Hirschmann, 2002; Pertermann et al., 2004). Clinopyroxenes from the Xu-Huai eclogite and garnet clinopyroxenite xenoliths, suggested to represent residues left after partial melting of the foundered Archean NCC lower crust to form the adakitic magma, are low in Al<sub>2</sub>O<sub>3</sub> (6.9–9.8%) (Gao et al., 2004; Xu et al., 2006), and clinopyroxene from the Feixian basalts (in both cores and exteriors), also have low Al<sub>2</sub>O<sub>3</sub> (≤6.9%) (Table S5 in Supplementary online materials). Accordingly, partition coefficients given by Barth et al. (2002a) for low-Al<sub>2</sub>O<sub>3</sub> (7.3–10.3%) clinopyroxene are used, which are broadly similar to those for clinopyroxene with 8.3–10.3% Al<sub>2</sub>O<sub>3</sub> (Xiong, 2006). Experiments for high-Al<sub>2</sub>O<sub>3</sub> (12.5–19.9%) clinopyroxene (Pertermann and Hirschmann, 2002; Pertermann et al., 2004) give significantly lower partition coefficients and are not considered. (a) Chondrite normalized rare earth element (REE) patterns. Shaded field represents experimentally produced melts from eclogite (Rapp et al., 1991, 1999). Thick line box is field of Xinglonggou lavas, interpreted as melts from foundered eclogite that interacted with the mantle (Gao et al., 2004). REE patterns of melts in equilibrium with clinopyroxene cores fall into two groups; the dominant one is similar to those of eclogite melts, and the other (with fewer analyses) are even more fractionated, requiring more garnet in the source. (b) Plot of Sr to Y ratios against Y. Fields for tonalite–trondhjemite–granodiorite (TTG) and adakites and rocks from classical island arcs are from Martin et al. (2005). Melts in equilibrium with cpx cores (circles) have fractionated rare earth element distributions, no Eu anomalies, and high Sr/Y ratios, consistent with those of eclogite-derived adakitic melts.

isotope systems must first be considered. The Feixian picrites have very high MgO (12.7–14.6 wt.%), Sr and Nd concentrations (1500 ppm, 90 ppm, respectively) and uniform Sr and Nd isotopic compositions (Table 1; Table S1). The high Sr and Nd concentrations mean that these isotope systems that are normally very sensitive to crustal contamination of mantle-derived melts, are not sensitive indicators here. Although Os concentrations in the whole rock samples average about three times higher than typical continental crust (~0.15 vs. 0.05 ppb; Peucker-Ehrenbrink and Jahn, 2001), the contrast between typical mantle and crustal  $^{187}\text{Os}/^{188}\text{Os}$  might generate resolvable effects resulting from crustal contamination for Os isotopes. However, the high, relatively uniform MgO of the picrites, together with the lack of correlation between initial  $\gamma_{\text{Os}}$  and possible indicators of crustal contamination, such as  $\text{K}_2\text{O}$ , suggests that crustal contamination was not a dominant process in defining Os isotopic composition variability in the Feixian rocks.

In contrast to the Feixian picrites, the chemical and isotopic compositions of the Sihetun basalts are more variable and some geochemical characteristics may reflect the influence of some degree of crystal fractionation/and or crustal contamination, as suggested by positive correlations ( $r=0.71\text{--}0.93$ ) between Mg# and Cr–Ni, and negative correlations ( $r=-0.65$  to  $-0.80$ ) between Mg# and LREE. There are also correlations between  $\gamma_{\text{Os}}$  (125 Ma) and both  $\text{K}_2\text{O}$  and  $\text{Al}_2\text{O}_3$  ( $r=0.78$  and  $0.64$ , respectively) (Fig. S3), consistent with modest crustal contamination. However, there are no clear correlations between chemical indicators of crustal contamination and either Sr or Nd isotopic compositions. As with the Feixian picrites, this may be due to the relatively high concentrations of Sr and Nd in the basalts coupled with the lack of a major contrast in isotopic composition between the lavas and the crust through which they transited. The minor amount of Sr and Nd isotopic heterogeneity, thus, more likely reflects derivation of melts coming from mantle sources with slightly different isotopic compositions. For these reasons, the Sr and Nd isotopes in these lavas are interpreted here to reflect their source compositions. The variable Os isotopic compositions of the whole rock samples, however, likely reflect minor crustal contamination.

Because Nd and Sr are incompatible elements, their concentrations and isotopic compositions in the putative pyroxenitic sources of both the Feixian picrites and Sihetun basalts would likely be dominated by those of the hybridizing melts derived from eclogites rather than the affected peridotites (see mixing calculations given below). One important observation, therefore, is that the evolved Nd and Sr isotopic compositions of the picrites [ $\epsilon_{\text{Nd}}$  (119 Ma) =  $-13$ ,  $^{87}\text{Sr}/^{86}\text{Sr}$  (119 Ma) =  $0.7098\text{--}0.7099$ ] are distinct from those of the basalts [ $\epsilon_{\text{Nd}}$  (125 Ma) =  $-1.6$  to  $-2.4$ ,  $^{87}\text{Sr}/^{86}\text{Sr}$  (125 Ma) =  $0.7065\text{--}0.7099$ ]. This requires that there were at least two isotopically distinct eclogites that contributed melt to hybridize the two distinct mantle sources. Both sources were considerably more evolved than typical depleted MORB mantle at that time [ $\epsilon_{\text{Nd}}$  (125 Ma) =  $+7$  to  $+10$ ;  $^{87}\text{Sr}/^{86}\text{Sr}$  (125 Ma) =  $0.702$  to  $0.704$ , Hoffmann (1997)]. Thus, the hypothesized eclogitic sources of the melts could not have been contemporary subducted slab components. Instead, the mantle sources of the picrites and basalts were likely hybridized by melt from eclogites that originated as ancient continental crust. We consider the most likely source of the eclogites to be foundered mafic lower continental crust that originated from the base of the NCC.

In contrast to Sr and Nd, Os isotopes are more sensitive to the proportion of eclogite-derived melt to peridotite in the hybridized sources. This conclusion is based on the assumptions that the putative foundered crustal eclogites and their derivative melts had low Os concentrations, and highly radiogenic Os isotopic compositions, and that the affected peridotites most likely had near-chondritic Os isotopic compositions but high Os concentrations. While it is impossible to precisely estimate the Os isotopic composition of eclogites that formed as lower continental crust in the NCC, a relatively robust estimate can be made using Re and Os concentrations typical of lower crustal or eclogite xenoliths worldwide (e.g., Esperanza et al., 1997; Saal et al., 1998; Barth et al., 2002b). Here, we assume Re and Os

concentrations of 1 and 0.078 ppb, respectively (well within the range of reported concentration data for mafic, lower crustal xenoliths). Using these concentrations, after 2.8 Ga the eclogites would have  $^{187}\text{Os}/^{188}\text{Os}$  of 4.88 ( $\gamma_{\text{Os}}$  (120) =  $+3750$ ), assuming evolution from a source with chondritic  $^{187}\text{Os}/^{188}\text{Os}$ .

In order to constrain the proportion of eclogite-derived melt in the mantle sources of the picrites and basalts, we calculate the Os–Nd isotope compositions of hybridized sources produced by mixing peridotite and an adakitic melt derived from partial melting of foundered eclogite. To do this we must first estimate the  $^{187}\text{Os}/^{188}\text{Os}$  of the mantle sources of the basalts and picrites. The  $>50$  unit spread in initial  $\gamma_{\text{Os}}$  for the Sihetun basalts cannot be attributed to error magnification resulting from age corrections (as is common for all but the youngest basalts), as Re/Os ratios for these basalts are relatively low. The relatively low Re/Os ratios also mean that recent Re loss is not likely to have caused variability in calculated initial ratios. Greater than 90% Re loss would be required to change initial  $\gamma_{\text{Os}}$  values by more than 10 units. Rather, the above-mentioned correlations between  $\gamma_{\text{Os}}$  (125 Ma) and  $\text{K}_2\text{O}$  and  $\text{Al}_2\text{O}_3$ , suggest that at least some of the variability may reflect modest crustal contamination.

The best constraint on the Os isotopic composition of the mantle source of these rocks must thus come from the chromite analyses. The modest variability in the Os isotopic compositions of the chromite separates likely reflects either: 1) partial re-equilibration of Os contained within the chromite phenocrysts with crustally contaminated magma at shallow depths, or 2) incorporation of some xenocrystic chromite in the separates. We assume that chromite xenocrysts derived from the peridotitic portion of the hybridized mantle source would have chondritic or subchondritic  $^{187}\text{Os}/^{188}\text{Os}$  at the time of eruption. We cannot discriminate between these two possibilities. Nevertheless, the consistency of the values argues that the mantle source composition was at least similar to the chromite compositions. A  $\gamma_{\text{Os}}$  (125 Ma) value of  $+17$  is henceforth taken as the value for the hybridized mantle source, as it is the lowest value for the Sihetun chromites. This value can be achieved in an ancient lithospheric mantle source by addition of a highly radiogenic adakitic melt as previously anticipated.

We now consider Os–Nd mixing of ancient lithospheric mantle (solid star on Fig. 8, assuming a 2.8 Ga melt extraction age, 3.7 ppb Os,

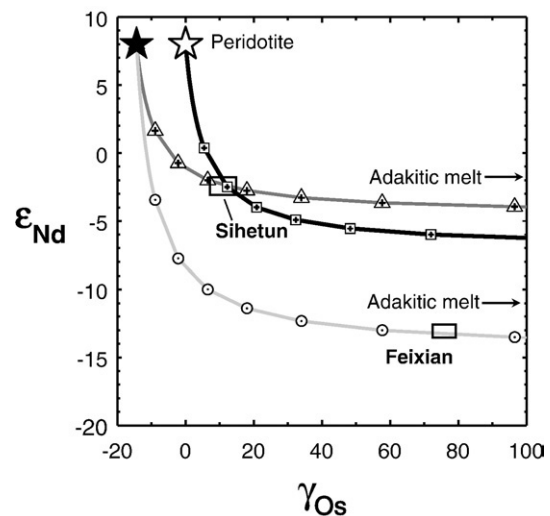


**Fig. 8.**  $\gamma_{\text{Os}}$  versus  $\epsilon_{\text{Nd}}$  mixing diagram for silicic melt–peridotite mixtures as discussed in the text. Starting peridotite compositions are shown as stars. Solid star reflects ancient NCC peridotite ( $\gamma_{\text{Os}} = -14.5$ , 3.7 ppb Os;  $\epsilon_{\text{Nd}} = +8$ , 3.0 ppm Nd). Open star is peridotite with chondritic Os isotopes and same concentrations and Nd isotopes as ancient peridotite. Starting adakitic melt compositions for the models are beyond the scale of the figure. Assumed melt compositions are as follows: black curve:  $\gamma_{\text{Os}} = +3756$ , 0.078 ppb Os;  $\epsilon_{\text{Nd}} = -4.5$ , 28 ppm Nd; dark gray curve:  $\gamma_{\text{Os}} = +3756$ , 0.078 ppb Os;  $\epsilon_{\text{Nd}} = -14.5$ , 28 ppm Nd. Triangles, squares and circles show increments of 10% mixing of melt into peridotite. Boxes show estimated compositions of Sihetun basalt and Feixian picrite sources.

$^{187}\text{Os}/^{188}\text{Os}=0.1083$ ,  $\gamma_{\text{Os}}(125\text{ Ma})=-14.5$ ,  $\epsilon_{\text{Nd}}=+8$ ,  $\text{Nd}=3.0\text{ ppm}$ ), with melt derived from equally ancient eclogite. The concentration of Os in the putative adakitic melt is difficult to estimate, but it is unlikely to have been substantially higher or lower than that of its eclogitic source. For mixing calculations we assume this melt had 0.078 ppb Os (the same as the parental eclogite, as discussed above),  $^{187}\text{Os}/^{188}\text{Os}=4.88$  or  $\gamma_{\text{Os}}(125\text{ Ma})=+3750$ , along with  $\epsilon_{\text{Nd}}=-4.5$  and  $\text{Nd}=28\text{ ppm}$ . Melt–peridotite mixtures would have  $\gamma_{\text{Os}}(125\text{ Ma})$  and  $\epsilon_{\text{Nd}}$  values appropriate for our estimate of the parental melts to the Sihetun basalts after 30–40% addition of the adakitic component (Fig. 8). A similar calculation assuming a chondritic  $^{187}\text{Os}/^{188}\text{Os}$  in the peridotite at the time of basalt formation (open star on Fig. 8), instead suggests the presence of only ~20% of the adakitic component in the mantle source (Fig. 8).

The initial Os isotopic composition of the Feixian picrites is difficult to constrain at present. The substantially different calculated initial  $^{187}\text{Os}/^{188}\text{Os}$  ratios of whole rock samples could be the result of crustal contamination, isotopically heterogeneous mantle sources, or heterogeneity due to variable incorporation of xenocrystic phases with substantially different isotopic compositions. There is no strong evidence of crustal contamination for this suite, but as with the basalts, typically sensitive indicators of crustal contamination, such as Nd and Sr isotopes, would not have been sensitive here because of their high concentrations in the melt. Consequently, crustal contamination cannot be ruled out, although the high Ni contents of the samples limit any crustal contamination to <10%. The outcrop area of the picrites is small, and probably contains only a few discrete flows, so the likelihood of sampling mantle heterogeneities seems low. The fact the two chromite separates have much lower initial Os isotopic compositions compared to the bulk samples suggests that the differences may be due to the variable presence of xenocrystic chromite that did not equilibrate with the surrounding melt. The paucity of chromite in these rocks suggests that, unlike for the Sihetun basalts, the chromites are likely not representative of the hybridized mantle source. We speculate that they are more representative of the pre-hybridized mantle. The relative uniformity of  $\gamma_{\text{Os}}$  values of bulk samples (averaging ~+76 if SFX-30 is not included) suggests that the parental liquid may have had a substantially more radiogenic initial Os isotopic composition than the Sihetun basalts. For modelling purposes, we assume a  $\gamma_{\text{Os}}(119\text{ Ma})=+76$ . This radiogenic value is also consistent with the more evolved  $\epsilon_{\text{Nd}}$  values of the Feixian picrites compared to those of the Sihetun basalts.

Using the same Os and Nd concentration and Os isotopic composition parameters used above for modelling the Sihetun basalt source, but assuming an  $\epsilon_{\text{Nd}}$  value of -14.5 for the adakite melt results in a mixing curve that passes through the estimated parental melt composition of the Feixian picrites with ~62% addition of the adakitic melt component to ancient NCC peridotite (Fig. 8). The low  $\epsilon_{\text{Nd}}$  value of -14.5 is required for any reasonable Nd concentrations, so the source of the Feixian picrites must have been modified by an adakitic melt with a substantially lower  $\epsilon_{\text{Nd}}$  value than that which modified the source of the Sihetun basalts. The assumption of an NCC peridotite end member for this mixing calculation is consistent with the abundant, forsteritic olivine xenocrysts and the low  $\gamma_{\text{Os}}$  chromites in these picrites.

### 6.5. Recycling of the deep lithosphere of the North China craton and implications for the source regions of mantle-derived basalts

From the above lines of evidence we propose that these Early Cretaceous picrites and high-Mg basalts formed by melting of peridotitic mantle that was hybridized by melts derived from a foundered Archean eclogitic lower crust (Gao et al., 2004) to form a pyroxenitic source. In the case of the Feixian picrites, the peridotite was likely derived from refractory lithospheric mantle of the North China craton, given the olivine xenocrysts of  $\text{Fo}_{>92}$  and the evidence in

the Os isotopes for an ancient, refractory component. Because eclogite is denser than peridotite (Rudnick and Fountain, 1995; Anderson, 2006; Levander et al., 2006), the eclogite would sink more rapidly than the more buoyant peridotite, and the eclogite melt would react to varying degrees with the Archean peridotitic mantle through which it ascends. This interaction would have converted olivine into pyroxene and lowered the melting temperature of the hybridized mantle (Yaxley and Green, 1998; Rapp et al., 1999; Yaxley, 2000; Sobolev et al., 2005, 2007; Herzberg, 2006), which subsequently melted to produce the Early Cretaceous alkaline picrites and high-Mg basalts. The reversely zoned clinopyroxenes may have formed in two ways. In both scenarios the cores crystallized from an eclogite-derived melt at high pressure and the exteriors grew at lower pressures. In the first scenario, the cores represent relicts that survived the peridotite hybridization process [clinopyroxene is a stable phase in hybridized peridotite (Yaxley and Green, 1998) and thus is difficult to dissolve]. These crystal cores would have been incorporated into the peridotite during hybridization and were subsequently overgrown during melting of the hybridized source to produce the basaltic magma. Alternatively, the clinopyroxenes could be the product of magma mixing within the mantle, where the cores crystallized from an eclogite-derived melt and the exteriors crystallized from a picritic magma derived from a hybridized source. This may explain complicated zoning in clinopyroxene from the Sihetun basalt. In either case, the eclogite-derived melt formed first at greater depths and triggered melting of the hybridized Archean mantle to form a basaltic or picritic magma at mantle pressures of 3–4 GPa.

Evidence for adakite interaction with ancient lithospheric mantle beneath the NCC during the Cretaceous also comes from mantle xenoliths from the Laiwu (also called Tietonggou) high-Mg diorite, which has adakitic affinities and intruded ~130 Ma ago in Shandong Province (Fig. 1) (Chen and Zhou, 2006; Yang et al., 2006). Here, dunite xenoliths are cut by orthopyroxene veins (Chen and Zhou, 2006; Xu et al., 2008), which contain secondary orthopyroxene, with or without Na-rich plagioclase, amphibole and phlogopite. The adakite–peridotite reaction consumed olivine and clinopyroxene in the surrounding peridotite. These veins were interpreted to mark the passage of adakitic melt through refractory peridotite shortly before emplacement of the host diorite (Chen and Zhou, 2006; Xu et al., 2008). Osmium isotopic compositions ( $^{187}\text{Os}/^{186}\text{Os}=0.1098\text{--}0.1104$ ) of three peridotite xenoliths from Laiwu yield Archean Re depletion model ages ( $T_{\text{RD}}=2600\text{--}2700\text{ Ma}$ , Table S9), which, like the highly forsteritic olivine cores in the Feixian picrites, document the presence of Archean lithospheric mantle beneath Shandong during the Early Cretaceous. These metasomatized peridotite and pyroxenite xenoliths have evolved Sr–Nd isotopic compositions [ $^{87}\text{Sr}/^{86}\text{Sr}(130\text{ Ma})=0.7062$ ,  $\epsilon_{\text{Nd}}(130\text{ Ma})=-6.9$ ], overlapping those of the Laiwu high-Mg diorite (Chen and Zhou, 2006). As mentioned above, the great enrichment in Sr and Nd in metasomatic melts compared to the lithospheric mantle means that the isotopic compositions of the metasomatized mantle should reflect that of the metasomatic agent, which, in this case, is similar to the Laiwu dioritic magma. Thus the Laiwu samples document overprinting of Archean lithospheric mantle by adakitic melts having evolved Sr–Nd isotopic compositions during the Early Cretaceous (Xu et al., 2008).

The Laiwu and other nearby high-Mg diorites [(Mg# = 63–67, Cr = 363–718 ppm, Yb = 1.1–1.7 ppm, Sr/Y = 30–43, Eu/Eu\* = 0.93–1.00,  $\epsilon_{\text{Nd}}=-4$  to -13 at 130 Ma (Yang et al., 2006; W.L. Xu, unpubl.)] are compositionally similar to the Xu-Huai high-Mg diorite that carries eclogite xenoliths in the southern NCC (Fig. 1) (Gao et al., 2004; Xu et al., 2006). The Xu-Huai diorite is also Early Cretaceous in age, contains inherited Archean zircons and is high-Mg and adakitic, with evolved Sr–Nd isotopic composition (Gao et al., 2004; Xu et al., 2006). The Xu-Huai high-Mg diorite is thus compositionally complementary to its entrained eclogite xenoliths (Xu et al., 2006). These geochemical and isotopic features are shared by the Early Mesozoic Xinglonggou high-Mg adakitic lavas (Gao et al., 2004). We thus suggest that, like the

Xinglonggou lavas (Gao et al., 2004), the Xu-Huai and Laiwu high-Mg diorites derived from partial melting of foundered eclogite, followed by interaction of that melt with the overlying mantle (Xu et al., 2006).

If the above interpretations are correct, they imply that thermochemical erosion of the Archean lithospheric mantle by upwelling asthenosphere (Menziez et al., 1993; Griffin et al., 1998; Menziez et al., 2007) or transformation of lithospheric to asthenospheric mantle by addition of melts (Zhang et al., 2007) or melts and water from a subducting slab (Niu, 2005) are not solely responsible for the destruction of the NCC Archean keel. None of these processes can explain the production of adakitic/TTG lavas from foundered NCC crust prior to basaltic magmatism, as observed in the Xinglonggou lavas from the Liaoning area, and as inferred from reversely zoned clinopyroxenes and other lines of evidence for mantle hybridization by eclogite-derived melts discussed above. Nor can these processes explain entrainment of fragments of the Archean mantle by high-Mg diorites of NCC crustal origin, as seen at Laiwu. Moreover, pyroxenite sources are not produced in the thermal–chemical erosion model.

These observations further suggest that recycling of the deep lithosphere (lower crust plus lithospheric mantle) of the North China craton initiated at least by the Early Mesozoic and lasted into the Early Cretaceous. This seemingly protracted period of foundering is consistent with numerical models that show that the removal of a 250 km thick lithospheric root takes between 55 and 750 Ma, depending on the root width and the viscosity contrast between the root and ambient mantle, as well as other parameters (Morency et al., 2002).

According to the above observations, the evolved Nd, Sr and Os isotopic compositions of the Mesozoic picrites and basalts derive from foundered eclogitic lower crust. Such an origin is consistent with evidence for the genesis of other foundering-induced basalts (Lustrino, 2005), and suggests that, as inferred for some ocean island basalts (Escrig et al., 2004; Lustrino, 2005; Sobolev et al., 2005; Anderson, 2006; Sobolev et al., 2007), eclogites of low melting temperatures may play an important role in modification, melting and melt productivity of intraplate, and possibly also mid-ocean ridge (Kamenetsky et al., 2001) basaltic source regions in the mantle.

## Acknowledgements

This research was supported by the National Nature Science Foundation of China (90714010, 40521001, 40673019, 40472033, 40672029), Chinese Ministry of Education (IRT0441, B07039 and 306021) and NSF (EAR 99031591 and EAR 0635671). We thank Claude Herzberg for the calculation of and very constructive discussion on the primary melt compositions and making Fig. 6a and H.Y. He, G.M. Shu, X.C. Wang, and H. Zhang for their help in Ar–Ar dating, electron microprobe and chemical and isotopic analysis as well as field work. We also thank Martin J. Streck for providing unpublished pyroxene data of high-Mg andesites from Mount Shasta. We finally thank Alex Sobolev and Marc Hirschmann for their review comments and Rick Carlson for editorial handling.

## Appendix A. Supplementary data

Supplementary data associated with this article can be found, in the online version, at doi:10.1016/j.epsl.2008.03.008.

## References

- Anderson, D.A., 2006. Speculations on the nature and cause of mantle heterogeneity. *Tectonophysics* 146, 7–22.
- Arndt, N.T., Goldstein, S.L., 1989. An open boundary between lower continental crust and mantle: its role in crust formation and crustal recycling. *Tectonophysics* 161, 201–212.
- Barnes, S.J., Roeder, P.L., 2001. The range of spinel compositions in terrestrial mafic and ultramafic rocks. *J. Petrol.* 42, 2279–2302.
- Barth, M.G., Foley, S.F., Horn, I., 2002a. Partial melting in Archean subduction zones: constraints from experimentally determined trace element partition coefficients between eclogitic minerals and tonalitic melts under upper mantle conditions. *Precambrian Res.* 113, 323–340.
- Barth, M.G., Rudnick, R.L., Carlson, R.W., Horn, I., McDonough, W.F., 2002b. Re–Os and U–Pb geochronological constraints on the eclogite–tonalite connection in the Archean Man Shield, West Africa. *Precambrian Res.* 118, 267–283.
- Chen, L.H., Zhou, X.H., 2006. Subduction-related metasomatism in the thinning lithosphere: evidence from a composite dunite–orthopyroxenite xenolith entrained in Mesozoic Laiwu high-Mg diorite, North China Craton. *Geochem. Geophys. Geosyst.* 6, Q06008. doi:10.1029/2005GC000938.
- Chen, L., Zheng, T.Y., Xu, W.W., 2006. A thinned lithospheric image of the Tanlu Fault Zone, eastern China: constructed from wave equation based receiver function migration. *J. Geophys. Res.* 111. doi:10.1029/2005JB003974.
- Elkins-Tanton, L.T., 2005. Continental magmatism caused by lithospheric delamination. In: Foulger, G.R., Natland, J.H., Presnall, D.C., Anderson, D.L. (Eds.), *Plates, Plumes, and Paradigms*. *Geol. Soc. Am. Spec. Pap.*, vol. 388, pp. 449–462.
- Escrig, S., Capmas, F., Dupré, B., Allégre, C.J., 2004. Osmium isotopic constraints on the nature of the DUPAL anomaly from Indian mid-ocean-ridge basalts. *Nature* 431, 59–63.
- Esperanca, S., Carlson, R.W., Shirey, S.B., Smith, D., 1997. Dating crust–mantle separation: Re–Os isotopic study of mafic xenoliths from central Arizona. *Geology* 25, 651–654.
- Gao, S., Luo, T.-C., Zhang, B.-R., Zhang, H.-F., Han, Y.-W., Hu, Y.-K., Zhao, Z.-D., 1998a. Chemical composition of the continental crust as revealed by studies in East China. *Geochim. Cosmochim. Acta* 62, 1959–1975.
- Gao, S., Zhang, B.-R., Jin, Z.-M., Kern, H., Luo, T.-C., Zhao, Z.-D., 1998b. How mafic is the lower continental crust? *Earth Planet. Sci. Lett.* 161, 101–117.
- Gao, S., Rudnick, R.L., Carlson, R.W., McDonough, W.F., Liu, Y.S., 2002. Re–Os evidence for replacement of ancient mantle lithosphere beneath the North China Craton. *Earth Planet. Sci. Lett.* 198, 307–322.
- Gao, S., Rudnick, R.L., Yuan, H.-L., Liu, X.-M., Liu, Y.-S., Xu, W.-L., Ling, W.-L., Ayers, J., Wang, X.-C., Wang, Q.-H., 2004. Recycling lower continental crust in the North China craton. *Nature* 432, 892–897.
- Griffin, W.L., Zhang, A.D., O'Reilly, S.Y., Ryan, C.G., 1998. Phanerozoic evolution of the lithosphere beneath the Sino-Korean Craton. In: Flower, M., Chung, S.-L., Lo, C.-H., Lee, T.-Y. (Eds.), *Mantle Dynamics and Plate Interactions in East Asia*. American Geophysical Union, Washington, DC, pp. 107–126.
- Guo, F., Nakamura, E., Fan, W.M., Kobayoshi, K., Li, C.W., 2007. Generation of Palaeocene adakitic andesites by magma mixing, Yanji Area, NE China. *J. Petrol.* 80, 1–32.
- Herzberg, C., 2006. Petrology and thermal structure of the Hawaiian plume from Mauna Kea volcano. *Nature* 444, 605–609.
- Herzberg, C., Asimow, P.D., Arndt, N., Niu, Y., Leshner, C.M., Fitton, J.G., Cheadle, M.J., Saunders, A.D., 2007. Temperatures in ambient mantle and plumes: constraints from basalts, picrites, and komatiites. *Geochem. Geophys. Geosyst.* 8, Q02006. doi:10.1029/2006GC001390.
- Hirschmann, M.M., Stolper, E.M., 1996. A possible role for garnet pyroxenite in the origin of the 'garnet signature' in MORB. *Contrib. Mineral. Petrol.* 124, 185–208.
- Hoffmann, A.W., 1997. Mantle geochemistry: the message from oceanic volcanism. *Nature* 385, 219–228.
- Hofmann, A.W., White, W.M., 1982. Mantle plumes from ancient oceanic crust. *Earth Planet. Sci. Lett.* 57, 421–436.
- Huang, F., Li, S., Yang, W., 2007. Contributions of the lower crust to Mesozoic mantle-derived mafic rocks from the North China Craton: implications for lithospheric thinning. In: Zhai, M.-G., Windley, B.F., Kusky, T.M., Meng, Q.R. (Eds.), *Mesozoic Sub-Continental Lithospheric Thinning under Eastern Asian*. *Geol. Soc. London Spec. Pub.*, vol. 280, pp. 55–75.
- Jull, M., Kelemen, P.B., 2001. On the conditions for lower crustal convective instability. *J. Geophys. Res.* 106, 6423–6446.
- Kamenetsky, V.S., Maas, R., Sushchevskaya, N.M., Norman, M.D., Cartwright, I., Peyve, A.A., 2001. Remnants of Gondwanan continental lithosphere in oceanic upper mantle: evidence from the South Atlantic Ridge. *Geology* 29, 243–246.
- Kamenetsky, V.S., Elburg, M., Arculus, R., Thomas, R., 2006. Magmatic origin of low-Ca olivine in subduction-related magmas: co-existence of contrasting magmas. *Chem. Geol.* 233, 346–357.
- Kay, R.W., Kay, S.M., 1991. Creation and destruction of lower continental crust. *Geol. Rundsch.* 80, 259–278.
- Kogiso, T., Hirschmann, M.M., 2001. Experimental study of clinopyroxenite partial melting and the origin of ultra-calcic melt inclusions. *Contrib. Mineral. Petrol.* 142, 347–360.
- Kogiso, T., Hirschmann, M.M., Frost, D.J., 2003. High-pressure partial melting of garnet pyroxenite: possible mafic lithologies in the source of ocean island basalts. *Earth Planet. Sci. Lett.* 216, 603–617.
- Lee, S.Y., Walker, R.J., 2006. Re–Os isotope systematics of mantle xenoliths from South Korea: evidence for complex growth and loss of lithospheric mantle beneath East Asia. *Chem. Geol.* 231, 90–101.
- Levander, A., Niu, F., Lee, C.-T.A., Cheng, X., 2006. Imaging the continental lithosphere. *Tectonophysics* 416, 167–185.
- Ling, W.L., Xie, X.J., Liu, X.M., Cheng, J.P., 2006. Zircon U–Pb dating on the Mesozoic volcanic suite from the Qingshan Group stratotype section in eastern Shandong Province and its tectonic significance. *Sci. China (D)* 36, 401–411 (in Chinese).
- Liou, J.G., Zhang, R.Y., Ernst, W.G., Rumble III, D., Maruyama, S., 1998. High pressure minerals from deeply subducted metamorphic rocks. *Rev. Miner.* 37, 33–96.
- Liu, D.-Y., Nutman, A.P., Compston, W., Wu, J.S., Shen, Q.-H., 1992. Remnants of >3800 Ma crust in the Chinese part of the Sino-Korean craton. *Geology* 20, 339–342.
- Lustrino, M., 2005. How the delamination and detachment of lower crust can influence basaltic magmatism. *Earth-Sci. Rev.* 72, 21–38.

- Martin, H., Smithies, R.H., Rapp, R., Moyen, J.-F., Champion, D., 2005. An overview of adakite, tonalite–trondhjemite–granodiorite (TTG), and sanukitoid: relationships and some implications for crustal evolution. *Lithos* 79, 1–24.
- McKenzie, D., O'Nions, R.K., 1983. Mantle reservoirs and oceanic basalts. *Nature* 301, 229–231.
- Menzies, M.A., Fan, W.-M., Zhang, M., 1993. Paleozoic and Cenozoic lithoprobes and the loss of > 120 km of Archean lithosphere, Sino-Korean craton, China. In: Prichard, H.M., Alabaster, T., Harris, N.B.W., Neary, C.R. (Eds.), *Magmatic Processes and Plate Tectonics*. Geol. Soc. London Spec. Pub., vol. 76, pp. 71–81.
- Menzies, M.A., Xu, Y., Zhang, H., Fan, W., 2007. Integration of geology, geophysics and geochemistry: a key to understanding the North China Craton. *Lithos* 96, 1–21.
- Morency, C., Doin, M.-P., Dumoulin, C., 2002. Convective destabilization of a thickened continental lithosphere. *Earth Planet. Sci. Lett.* 202, 303–320.
- Niu, Y.L., 2005. Generation and evolution of basaltic magmas: some basic concepts and a new view on the origin of Mesozoic–Cenozoic basaltic volcanism in Eastern China. *Geol. J. China Univ.* 11, 9–46.
- Pearson, D.G., Canil, D., Shirey, S.B., 2003. Mantle samples included in volcanic rocks: xenoliths and diamonds. In: Carlson, R.W. (Ed.), *Treatise on Geochemistry*, vol. 2, The Mantle and Core. Elsevier, pp. 172–275.
- Pei, F.P., Xu, W.L., Wang, Q.H., Wang, D.Y., Lin, J.Q., 2004. Mesozoic basalt and mineral chemistry of the mantle-derived xenocrysts in Feixian, Western Shandong, China: constraints on nature of Mesozoic lithospheric mantle. *Geol. J. China Univ.* 10, 88–96 (in Chinese).
- Pertermann, M., Hirschmann, M.M., 2002. Trace-element partitioning between vacancy-rich eclogitic clinopyroxene and silicate melt. *Am. Mineral.* 87, 1365–1376.
- Pertermann, M., Hirschmann, M.M., Hametner, K., Günther, D., Schmidt, M.W., 2004. Experimental determination of trace element partitioning between garnet and silica-rich liquid during anhydrous partial melting of MORB-like eclogite. *Geochem. Geophys. Geosyst.* 5, Q05A01. doi:10.1029/2003GC000638.
- Peucker-Ehrenbrink, B., Jahn, B.-m., 2001. Rhenium–osmium isotope systematics and platinum group element concentrations: loess and the upper continental crust. *Geochem. Geophys. Geosyst.* 2, 2001GC000172.
- Pilet, S., Hernandez, J., Villament, B., 2002. Evidence for high silicic melt circulation and metasomatic events in the mantle beneath alkaline provinces: the Na–Fe–augitic green-core pyroxenes in the Tertiary alkali basalts of the Cantal massif (French Massif Central). *Mineral. Petrol.* 76, 39–72.
- Pilet, S., Hernandez, J., Bussy, F., Sylvester, P.J., Poujol, M., 2005. The metasomatic alternative for ocean island basalt chemical heterogeneity. *Earth Planet. Sci. Lett.* 236, 148–166.
- Rapp, R.P., Watson, E.B., Miller, C.F., 1991. Partial melting of amphibolite/eclogite and the origin of Archean trondhjemites and tonalites. *Precambrian Res.* 51, 1–25.
- Rapp, R.P., Shimizu, N., Norman, M.D., Applegate, G.S., 1999. Reaction between slab-derived melts and peridotite in the mantle wedge: experimental constraints at 3.8 GPa. *Chem. Geol.* 160, 335–356.
- Roeder, P.L., Emslie, R.F., 1970. Olivine–liquid equilibrium. *Contrib. Mineral. Petrol.* 29, 275–289.
- Rudnick, R.L., Fountain, D.M., 1995. Nature and composition of the continental crust: a lower crustal perspective. *Rev. Geophys.* 33, 267–309.
- Rudnick, R.L., Gao, S., 2003. Composition of the continental crust. In: Rudnick, R.L. (Ed.), *Treatise on Geochemistry*, vol. 3, The Crust. Elsevier, pp. 1–64.
- Rudnick, R.L., Gao, S., Ling, W.L., Liu, Y.S., McDonough, W.F., 2004. Petrology and geochemistry of spinel peridotite xenoliths from Hannuoba and Qixia, North China Craton. *Lithos* 77, 609–637.
- Saal, A.E., Rudnick, R.L., Ravizza, G.E., Hart, S.R., 1998. Re–Os isotope evidence for the composition, formation and age of the lower continental crust. *Nature* 393, 58–61.
- Shirey, S.B., Walker, R.J., 1998. The Re–Os isotope system in cosmochemistry and high-temperature geochemistry. *Annu. Rev. Earth Planet. Sci.* 26, 423–500.
- Skjerlie, K.P., Patino Douce, A.E., 2002. The fluid-absent partial melting of a zoisite-bearing quartz eclogite from 1.0 to 3.2 GPa: implications for melting in thickened continental crust and for subduction-zone processes. *J. Petrol.* 39, 29–60.
- Sobolev, A.V., Hofmann, A.W., Sobolev, S.V., Nikogosian, I.K., 2005. An olivine-free mantle source of Hawaiian shield basalts. *Nature* 434, 590–597.
- Sobolev, A.V., et al., 2007. The amount of recycled crust in sources of mantle-derived melts. *Science* 316, 412–417.
- Streck, M.J., Leeman, W.P., Chesley, J., 2007. High-magnesian andesite from Mount Shasta: a product of magma mixing and contamination, not a primitive mantle melt. *Geology* 35, 351–354.
- Thompson, R.N., Gibson, S.A., 2000. Transient high temperatures in mantle plume heads inferred from magnesian olivines in Phanerozoic picrites. *Nature* 407, 502–506.
- Toplis, M.J., 2005. The thermodynamics of iron and magnesium partitioning between olivine and liquid: criteria for assessing and predicting equilibrium in natural and experimental systems. *Contrib. Mineral. Petrol.* 149, 22–39.
- Walker, R.J., Prichard, H.M., Ishiwatari, A., Pimentel, M., 2002. The osmium isotopic composition of convecting upper mantle deduced from ophiolite chromitites. *Geochim. Cosmochim. Acta* 66, 329–345.
- Wang, X.R., Gao, S., Liu, X.M., Yuan, H.L., Hu, Z.C., Zhang, H., Wang, X.C., 2006. Geochemistry of high-Mg andesites from the early Cretaceous Yixian Formation, western Liaoning: implications for lower crustal delamination and Sr/Y variations. *Sci. China (D)* 49, 904–914.
- Wu, F.Y., Walker, R.J., Ren, X.W., Sun, D.Y., Zhou, X.H., 2003. Osmium isotopic constraints on the age of lithospheric mantle beneath northeastern China. *Chem. Geol.* 197, 107–129.
- Wu, F.Y., Lin, J.Q., Wilde, S.A., Zhang, X.O., Yang, J.H., 2005. Nature and significance of the Early Cretaceous giant igneous event in eastern China. *Earth Planet. Sci. Lett.* 233, 103–119.
- Wu, F.Y., Walker, R.J., Yang, Y.H., Yuan, H.L., Yang, J.H., 2006. The chemical–temporal evolution of lithospheric mantle underlying the North China Craton. *Geochim. Cosmochim. Acta* 70, 5013–5034.
- Xiong, X.L., 2006. Trace element evidence for growth of early continental crust by melting of rutile-bearing hydrous eclogite. *Geology* 34, 945–948.
- Xu, Y.G., 2001. Thermo-tectonic destruction of the Archean lithospheric keel beneath the Sino-Korean Craton in China: evidence, timing and mechanism. *Phys. Chem. Earth (A)* 26, 747–757.
- Xu, W.L., Gao, S., Wang, Q.-H., Wang, D.Y., Liu, Y.S., 2006. Mesozoic crustal thickening of the eastern North China Craton: evidence from eclogite xenoliths and petrologic implications. *Geology* 34, 721–724.
- Xu, W.L., Hergt, J.M., Gao, S., Pei, F.P., Wang, W., Yang, D.P., 2008. Interaction of adakitic melt–peridotite: implications for the high-Mg# signature of Mesozoic adakitic rocks in the eastern North China Craton. *Earth Planet. Sci. Lett.* 265, 123–137.
- Yang, C.H., Xu, W.L., Yang, D.P., Liu, C.C., Liu, X.M., Hu, Z.C., 2006. Petrogenesis of the Mesozoic high-Mg diorites in West Shandong: geochronological and geochemical evidence. *Earth Sci.* 31, 81–92 (in Chinese).
- Yaxley, G.M., 2000. Experimental study of the phase and melting relations of homogeneous basalt plus peridotite mixtures and implications for the petrogenesis of flood basalts. *Contrib. Mineral. Petrol.* 139, 326–338.
- Yaxley, G.M., Green, D.H., 1998. Reactions between eclogite and peridotite: mantle refertilisation by subduction of oceanic crust. *Schweiz. Mineral. Petrogr. Mitt.* 78, 243–255.
- Zhang, H.-F., Ying, J.-F., Shimoda, G., Kita, N.T., Morishita, Y., Shao, J.-A., Tang, Y.-J., 2007. Importance of melt circulation and crust–mantle interaction in the lithospheric evolution beneath the North China Craton: evidence from Mesozoic basalt-borne clinopyroxene xenocrysts and pyroxenite xenoliths. *Lithos* 96, 67–89.
- Zhang, H.-F., Goldstein, S.L., Zhou, X.H., Sun, M., Zheng, J.-P., Cai, Y., 2008. Evolution of subcontinental lithospheric mantle beneath eastern China: Re–Os isotopic evidence from mantle xenoliths in Paleozoic kimberlites and Mesozoic basalts. *Contrib. Mineral. Petrol.* 155, 271–293.
- Zhao, G.C., Sun, M., Wilde, S.A., Li, S.Z., 2005. Late Archean to Paleoproterozoic evolution of the North China Craton: key issues revisited. *Precambrian Res.* 136, 177–202.
- Zheng, J.P., Griffin, W.L., O'Reilly, S.Y., Lu, F.X., Wang, C.Y., Zhang, M., Wang, F.Z., Li, H.M., 2004. 3.6 Ga lower crust in central China: new evidence on the assembly of the North China Craton. *Geology* 32, 229–232.
- Zheng, J.P., Griffin, W.L., O'Reilly, S.Y., Yang, J.S., Li, T.F., Zhang, M., Zhang, R.Y., Liou, J.G., 2006. Mineral chemistry of peridotites from Paleozoic, Mesozoic and Cenozoic lithosphere: constraints on mantle evolution beneath Eastern China. *J. Petrol.* 47, 2233–2256.
- Zhou, Z., Barrett, P.M., Hilton, J., 2003. An exceptionally preserved Lower Cretaceous ecosystem. *Nature* 421, 807–814.
- Zhu, R.X., Lo, C.-H., Shi, R.P., Shi, G.H., Pan, Y.X., Shao, J., 2004. Palaeointensities determined from the middle Cretaceous basalt in Liaoning Province, northeastern China. *Phys. Earth Planet. Inter.* 142, 49–59.